THOUGHTS ON TWO APPROACHES FOR ACCOUNTING FOR THE SCATTER IN FATIGUE DELAMINATION GROWTH CURVES

R. Jones[1], D. Peng[1], R. K Sing Raman[1], A. J. Kinloch[2] and J. Michopoulos[3]

[1]Centre of Expertise for Structural Mechanics, Department of Mechanical and Aerospace Engineering, Monash University, Clayton, Victoria, 3800, Australia.

[2]Department of Mechanical Engineering, Imperial College London, Exhibition Road, London SW7 2AZ, UK.

[3]Computational Multiphysics Systems Laboratory, Code 6394, Center for Materials Physics and Technology, US Naval Research Laboratory, Washington, DC 20375, United States.

ABSTRACT

This paper discusses two approaches that have been proposed to account for the data scatter observed in delamination growth tests under cyclic-fatigue loading and thereby enable an estimate of a worst-case delamination growth curve for use in the damage tolerance and durability assessment of composite and adhesively-bonded airframes. The two approaches discussed are: (a) the normalisation approach, whereby the energy release rate is divided by the resistance to delamination growth, $G_R(a)$, and (b) the Hartman-Schijve approach to delamination growth. It is shown that for the cases considered this normalisation approach can be used to yield curves that are similar to the 'mean-3σ', "worst-case", i.e. upper-bound, curve obtained using the Hartman-Schijve equation. However, despite the reduction in the scatter that arises if this particular normalisation approach is adopted, there is still considerable scatter in the important "near-threshold" region. In this region the normalised curves are bounded above by the 'mean-3σ' curve obtained using the Hartman-Schijve equation. To address this issue, an alternative normalisation approach is then proposed. This alternative normalisation approach has the advantage of having reduced scatter in the near-threshold region but elsewhere is significantly more conservative than the Hartman-Schijve approach.

Keywords: Delamination growth; durability and damage tolerance; scatter; Hartman-Schijve equation; normalisation

NOMENCLATURE

a	total crack (delamination) length, measured from the loading line
a_0	length of the initial delamination in the test specimen, i.e. the length of the (thin) film used as a starter crack, measured from the loading line
a_p	length of the pre-crack (pre-delamination), measured from the loading line, in the test specimen
a_p-a_0	pre-crack (pre-delamination) extension length in the test specimen
da/dN	rate of delamination growth per cycle
N	number of fatigue cycles
A	a constant in the Hartman-Schijve equation
D	a constant in the Hartman-Schijve equation
n	exponent in the Hartman-Schijve equation
G	energy release-rate
G_C	quasi-static interlaminar fracture energy
G_{C0}	quasi-static initiation value of G_C
$G_{fc}(a\text{-}a_0)$	the critical fatigue resistance increase as a function of the fatigue crack extension (a-a_0)
G_{max}	maximum value of the applied energy release-rate in the fatigue cycle
$G_{max.th}$	maximum value of the applied energy release-rate in the fatigue cycle at a value of da/dN of 10^{-10} m/cycle
G_{min}	minimum value of the applied energy release-rate in the fatigue cycle
$G_R(a)$	functional dependence of the quasi-static energy release rate on (a-a_p)
ΔG	range of the applied energy release-rate in the fatigue cycle, as defined below $\Delta G = G_{max} - G_{min}$
$\Delta\sqrt{G}$	range of the applied energy release-rate in the fatigue cycle, as defined below $\Delta\sqrt{G} = \sqrt{G_{max}} - \sqrt{G_{min}}$
$\Delta\sqrt{G_{th}}$	value of $\Delta\sqrt{G}$ at a value of da/dN of 10^{-10} m/cycle
$\Delta\sqrt{G_{thr}}$	range of the fatigue threshold value of $\Delta\sqrt{G}$, as defined below $\Delta\sqrt{G_{thr}} = \sqrt{G_{max.thr}} - \sqrt{G_{min.thr}}$
$\sqrt{G_{max.thr}}$	threshold value of $\sqrt{G_{max}}$
$\sqrt{G_{min.thr}}$	threshold value of $\sqrt{G_{min}}$
R	displacement or stress ratio
σ	standard deviation
CFRP	carbon-fibre reinforced-plastic

CT	compact tension specimen
DCB	double cantilever beam
DSTO	Defence Science and Technology Organisation
FCG	fatigue crack growth
JSSG-2006	Joint Services Specification Guidelines
MT	middle-tension specimen
NASA	National Aeronautics and Space Administration
SENT	single-edged notched tension specimen
US	United States
USAF	United States Airforce

1. INTRODUCTION

The damage tolerance and durability requirements associated with composite and bonded US military aircraft are delineated in the USAF certification standard MIL-STD-1530D [1] and the United States Joint Services Specification Guidelines JSSG-2006 [2], and guidelines for achieving these requirements are given in US Composite Materials Handbook CMN-17-3G [3]. The importance of determining the extensive scatter associated with the structural performance of a composite material is a key feature of [1-4]. In this context MIL-STD-1530D [1] explains that damage growth must be predictable and that the objectives of full-scale aircraft structure durability tests is to validate, or correct, the damage tolerance analysis. The question thus arises:

'How can we determine the necessary "worst-case", i.e. upper-bound, delamination curves needed to predict the growth of the fastest possible delamination?'

To this end, the present paper first discusses two approaches that have been proposed in the literature to estimate these worst-case curves. The two approaches compared are: (a) the normalisation approach, whereby the energy release-rate is divided by the resistance to delamination growth $G_R(a)$, and (b) the Hartman-Schijve approach to delamination growth.

This normalisation approach follows from the work of Poursartip [5] who was the first to suggest that delamination growth rate da/dN should be expressed as a function of $G_C/G_R(a)$, where $G_R(a)$ is the delamination resistance and is a function of both the delamination length and also the test procedure. This approach to representing delamination growth, which is entirely empirical, is now moderately widely used [e.g. 6-14], and has the advantage that it can

significantly reduce the data scatter. Murri [6] subsequently suggested that *da/dN* should be expressed as a function of $(G_{max}/G_R(a))G_{C0}$ where G_{C0} is the quasi-static initiation value of G_C. It can be argued that, since the *da*/*dN* versus G'_{max} (= $(G_{max}/G_R(a))G_{C0}$) curves essentially collapsed the experimentally-measured *da*/*dN* versus G_{max} curves, the upper-bound of the collapsed *da/dN* versus $(G_{max}/G_R(a))G_{C0}$ curves might well represent an approximate worst-case curve. Yao et al [11] suggested a variant of this approach whereby *da/dN* was expressed in the form:

$$da/dN = c\left[\frac{G_0\,\Delta\sqrt{G}}{G_{fC}(a-a_0)}\right]^m \tag{1}$$

where *c* and *m* are constants, G_0 is the fatigue delamination resistance with no fibre bridging, $G_{fc}(a\text{-}a_0)$ represents the critical resistance which increase with fatigue crack extension and

$$\Delta\sqrt{G} = \sqrt{G_{max}} - \sqrt{G_{min}} \tag{2}$$

This approach has the advantage that it takes into account the difference between the quasi-static crack resistance and the crack resistance that occurs during fatigue crack growth. Variants of this approach can be found in the papers by Gong and co-workers [15, 16], and a novel means for determining G_{fc} is given in [16].

On the other hand, the methodology presented in [17-19] for estimating this worst-case curve utilises the Hartman-Schijve crack growth equation. The Hartman-Schijve equation is a variant of the Nasgro equation [20-24] that for delamination/disbond growth can be written in the form:

$$da/dN = D\left[\frac{\Delta\sqrt{G}-\Delta\sqrt{G_{thr}}}{\sqrt{\{1-\sqrt{G_{max}}/\sqrt{A}\}}}\right]^n \tag{3}$$

Here D, n and A are constants and the value of A is often taken to be equivalent to the quasi-static value of the interlaminar fracture energy, G_C, or it may be fitted [17], and the term $\Delta\sqrt{G_{thr}}$ represents the fatigue threshold, see [17-22] for more details[1]. An advantage of this formulation is that not only can the scatter in the delamination growth data be captured and a worst-case ('mean-3σ') curve determined, but that anomalies that may arise when attempting to compute FCG under both constant and variable amplitude loading using formulations based on expressing da/dN as a function of G_{max}, or ΔG, disappear [4, 17-19, 45, 56].

As explained in [18], the term $\Delta\sqrt{G_{thr}}$ differs from the quantity $\Delta\sqrt{G_{th}}$, which corresponds to the value of $\Delta\sqrt{G}$ associated with a delamination growth rate, da/dN, of 10^{-10} m/cycle. The use of $\Delta\sqrt{G_{th}}$ in Equation (3) is inappropriate. Since, at $\Delta\sqrt{G} = \Delta\sqrt{G_{th}}$, then Equation (3) would return a value of da/dN that is zero instead of the required value of $da/dN = 10^{-10}$ m/cycle. Therefore, the term $\Delta\sqrt{G_{thr}}$ is introduced to ensure that at $\Delta\sqrt{G} = \Delta\sqrt{G_{th}}$ the value of da/dN is equal to 10^{-10} m/cycle. Hence, the values of $\Delta\sqrt{G_{thr}}$ and $\Delta\sqrt{G_{th}}$ are related by Equation (4), viz:

$$10^{-10} = D\left[\frac{\Delta\sqrt{G_{th}} - \Delta\sqrt{G_{thr}}}{\sqrt{\{1-\sqrt{G_{max}}/\sqrt{A}\}}}\right]^n \tag{4}$$

As indicated earlier a main purpose of the present paper is to investigate the relationship between the approach proposed by Murri [6] and the Hartman-Schijve methodology to estimating a worst-case curve. As a result of this study it is shown that, for the cases considered, the normalisation approach can be used to yield curves that are similar to the 'mean-3σ' curve obtained using the Hartman-Schijve equation. It is found also that despite the reduction in the

[1] Whilst the origin of Equation (3) can be traced back to Hartman and Schijve [23], similar equations can be found in [24-29]. A range of examples showing how this formulation can be used to study aircraft sustainment related problems are given in [30-38]. Applications to bridge steels and rail steels are given in [39-40], to composites materials [17-22, 41-44], structural adhesives in [4, 45-47], bonded wood joints [47], polymers [48] and to crack growth in granite [49]. Equation (3) has also been shown to hold for the growth of both long and small cracks in additively manufactured materials [50-54], as well as for crack growth in both laser additive and cold spray repairs to metallic structures [54,55].

scatter that arises if the normalisation approach is used, there is nevertheless considerable scatter remaining in the "near-threshold" region using this approach. It is also shown that, in the examples studied, in this region the normalised curves are bounded by the 'mean-3σ' curve obtained using the Hartman-Schijve equation.

Despite the fact that most composite and adhesively-bonded airframes are designed in accordance with a "no growth" design philosophy, there are now instances where disbonding and delaminations have been found to grow in operational aircraft. As a result there is now interest in allowing for slow delamination growth, and consequently in how to account for the near-threshold region. Consequently, an alternative normalisation approach, which is based on normalising with respect to the fatigue threshold, is also presented. In the examples presented in this paper it is found that this alternative approach has a reduced scatter in the near-threshold region, and therefore addresses the scattering in the "near-threshold" region that is seen in the original normalization approach. However, whilst this alternative approach has the advantage of having reduced scatter in the near-threshold region, at somewhat high fatigue crack growth (FCG) rates it is significantly more conservative than the worst-case, 'mean-3σ' curve deduced from the Hartman-Schijve methodology.

2. DELAMINATION GROWTH IN IM7/977-3 CFRP

The paper by Murri [6] presented da/dN versus G_{max} curves for delamination growth in a uni-directional IM7/977-3 CFRP DCB specimens tested at 90, 50, 40 and 30% of G_c, see Figure 1. (The subscript 'I' is added to note that we have a 'Mode I' (tensile opening) mode of fracture in the DCB test.) It was also shown that plotting da/dN as a function of G'_{max}, which Murri defined as $(G_{max}/G_R(a))G_{co}$, significantly reduced the scatter, as shown in Figure 2. As an alternative approach, a subsequent paper [17] revealed that the scatter in the data could be captured by the Hartman-Schijve variant of the Nasgro equation, i.e. Equation (5):

$$\frac{da}{dN} = 1.15 \text{ x} 10^{-9} \left[\frac{\sqrt{G_{max}} - \sqrt{G_{max.thr}}}{\sqrt{\{1 - \sqrt{G_{max}}/\sqrt{A}\}}} \right]^{2.24} \qquad (5)$$

with A = 154 J/m^2. It was also shown in [17] that the estimated worst-case (i.e. 'mean-3σ') curve corresponded to a threshold $\sqrt{G_{max.thr}}$ of approximately 4.79 $\sqrt{(}$J/m^2). This 'mean-3σ' curve is also shown in Figure 2. Here we see that the normalised curves are similar to, and are

bounded above, by the 'mean-3σ' curve presented in [17]. We also see that the scatter in the "normalised" curve is captured reasonably well by Equation (3) with threshold values for $\sqrt{G_{max.thr}}$ of 7.4, 6.1 and 5.9 $\sqrt{(J/m^2)}$.

3. DELAMINATION GROWTH IN M30SC/DT120 CFRP

The experimental results analysed in this section are associated with $R = 0.5$ DCB tests using the M30SC/DT120 CFRP laminates. The da/dN versus $\Delta\sqrt{G_I}$ curves can be seen in Figure 3. These curves have all been previously reported [57-61], and summarised in [18], where it was shown that delamination growth in these various tests could be expressed as per Equation (3) with the constants D and n as given in Table 1. The values of the delamination resistance term A used for each of these forty-six tests are given in [18]. The 'mean-3σ' upper-bound FCG curve determined in [18] for these tests is also shown in Figure 3. Yao et al. [62] subsequently presented da/dN versus $\Delta\sqrt{G_I}$ curves associated with delamination in multidirectional composite laminates M30SC/DT120, see Figure 4 which also contains the worst-case, 'mean-3σ', upper-bound FCG curve given in [18].

Yao et al. [62] also presented the normalised da/dN versus $(\Delta\sqrt{G'})^2$, where $\Delta\sqrt{G'} = (\Delta\sqrt{G}(\sqrt{(G_{C0}/G_R(a))}$. These curves are shown in Figure 5 where we again see that normalising in this fashion has significantly reduced the scatter. Figure 5 also contains the worst-case 'mean-3σ' FCG curve from the Hartman-Schijve methodology. Here we see that the normalised curves are similar to the 'mean-3σ' curve presented in [18]. Despite the reduction in the scatter obtained using this particular normalisation approach, Figures 2 and 5 still show considerable scatter in the "near-threshold" region. It is notable that the normalised curve associated with the pre-crack extension length, a_p-a_o, of 11.4 mm prior to the start of measurements from a DCB fatigue test in Figure 5 essentially coincides with the 'mean-3σ' curve given in [18].

4. DISCUSSION

The above sections have discussed two approaches that are being proposed to account for the scatter/variability seen in delamination/disbond fatigue crack growth tests in composites, and estimate a worst-case delamination growth curve for subsequent use in damage tolerance and durability analyses. The two approaches compared are (a) the normalisation approach whereby

the energy release rate is divided by the resistance to delamination growth $G_R(a)$ and (b) the Hartman-Schijve methodology to delamination growth. The two cases considered suggest that the normalisation approach can be used to yield curves that are similar to the 'mean-3σ' delamination growth curve obtained using the Hartman-Schijve equation. However, despite the reduction in the scatter that arises if this particular normalisation approach is adopted, there is nevertheless still considerable scatter in the "near-threshold" region. Given that, as detailed in the Composite Materials Design Handbook CMH-17-3G [3], most composite airframes are designed in accordance with a "no growth" design philosophy the next stage in the evolution of the use of composites in airframes involves the acceptance of slow growth. As such characterising delamination growth in the near-threshold region will be particularly important. Consequently, in the next section we will examine a normalisation technique, which attempts to minimise scatter in the near-threshold region.

5. OBSERVATIONS ON THE RELATIONSHIP BETWEEN *R* RATIO EFFECTS AND THE FATIGUE THRESHOLD NORMALISED STRESS INTENSITY FACTOR

5.1 Normalised crack growth curves for metallic structures

The paper by Schönbauer et al. [63] studied crack growth in 12% Cr martensitic stainless steel, which is one of the most prevalent blading materials used in low-pressure turbines, and suggested a different normalising approach. This study suggested that the crack growth curves could be normalised by dividing ΔK by the fatigue threshold ΔK_{th} and revealed that the various R ratio dependent da/dN versus ΔK curves collapsed when plotted as da/dN versus $\Delta K/\Delta K_{th}$. This finding also appears to hold for crack growth in the aluminium-alloy 7050-T7451, which is widely used in the F/A-18 (Classic Hornet) the F/A-18E/F (Super Hornet) and the F-35 (Joint Strike Fighter), see Figures 6 and 7 that contains data presented in [64]. The values of ΔK_{th} used in these various examples are given in Table 2.

Kujawski [65] presented the R ratio dependent da/dN versus ΔK curves for the aluminium alloy 2324-T39, see Figure 8. Now, Figure 9 reveals that when replotted in the form da/dN versus $\Delta K/\Delta K_{th}$ the R ratio dependency again essentially disappears and the various data sets collapse into one another. The values of ΔK_{th} used in Figure 9 are given in the Table 2. Kujawski [66] also presented the R ratio dependent da/dN versus ΔK curves for the aluminium-alloy 6013-T651, see Figure 10. Again, Figure 11 reveals that when replotted in the form da/dN versus

$\Delta K/\Delta K_{th}$ the R ratio dependency essentially disappears and the various data sets collapse. The values of ΔK_{th} used in Figure 11 are given in the Table 2.

The US Federal Aircraft Administration (FAA) data base [67] presents *da/dN* versus ΔK curves for AA 2024-T3 tested at R = -1.0, 0, 0.5 and 0.7, see Figure 12. In Figure 13 it is shown that when replotted in the form *da/dN* versus $\Delta K/\Delta K_{th}$ the R ratio dependency essentially disappears and the various data sets again collapse. The values of ΔK_{th} used in Figure 13 are given in Table 2.

Martelo et al. [68] presented R = 0.1 and 0.5 crack data for a cold-rolled metastable austenitic stainless steel, see Figure 14. Now, Figure 15 reveals that when replotted in the form of *da/dN* versus $\Delta K/\Delta K_{th}$ the R ratio dependency essentially disappears and the two data sets yet again collapse. The values of ΔK_{th} used in Figure 15 are also given in Table 2.

5.2. Anomalous crack growth curves

Kim et al. [69] reported an anomaly in that compact tension (CT) and single-edged notched tension (SENT) tests on 7075-T6511 and 7055-T6511 aluminium-alloy specimens gave different *da/dN* versus ΔK curves, see Figure 16. Jones et al. [70] reported that these differences could also be accounted for by considering the effect of the threshold values. Indeed, when these data sets are replotted in the form *da/dN* versus $\Delta K/\Delta K_{th}$ the anomalies disappear and the various data sets essentially collapse, see Figure 17. The values of ΔK_{th} used in Figure 17 are given in Table 2.

5.3. Crack growth in Additively Manufactured Inconel 625

Let us next consider crack growth in Additively Manufactured (AM) Inconel 625 alloy [71]. This paper presented the *da/dN* versus ΔK curves for AM Inconel 625 fabricated using selective layer melt (SLM) at R ratios of 0.1, 0.5 and 0.7. Curves were presented for FCG where crack growth was either parallel to the build direction or perpendicular to the build direction, see Figure 18. As shown in Figure 19 these various curves also collapse if *da/dN* is plotted against $\Delta K/\Delta K_{th}$. The values of ΔK_{th} used in Figure 19 are given in Table 3.

5.4 Remarks

The examples studied, which range from the aerospace aluminium-alloys 7050-T7451, 7075-T651, 7055-T651, 6013-T651, 2024-T3 and 2324-T39, a cold-rolled metastable austenitic stainless steel, and an additively manufactured Inconel 625 alloy reveal that when da/dN is expressed as a function of $\Delta K/\Delta K_{th}$ the R ratio dependency that is often seen when da/dN is plotted against ΔK essentially vanishes. Furthermore, other anomalies associated with da/dN versus ΔK curves reported in the literature are also shown to essentially vanish when the curves are replotted in the form da/dN versus $\Delta K/\Delta K_{th}$. *This finding suggests that for the cases studied these differences, e.g. the R ratio effects associated with the growth of long cracks, are merely reflections of the different thresholds associated with the various tests*. It also suggests an alternative, empirical, approach for normalising delamination growth curves in composite materials whereby $\Delta\sqrt{G}$ (or $\sqrt{G_{max}}$) is normalised by the threshold value $\Delta\sqrt{G_{th}}$ (or $\sqrt{G_{max.th}}$). Nevertheless, in the case of the composite materials, if we are to compare readily the results that we so obtain to the worst-case, 'mean-3σ', upper-bound curves calculated from the Hartman-Schijve methodology, then a somewhat more complex form of the term for the x-axis is needed than for the metallic materials. This aspect is discussed in the next section.

6. APPLICATION TO DELAMINATION GROWTH

6.1 Delamination growth in IM7/977-3 CFRP

To evaluate this alternative normalising approach then let us consider the IM7/977-3 CFRP curves presented in [6, 17] and reproduced in Figures 1 and 2. Now, Figure 20 presents plots of the da/dN versus G''_{max} ($=G_{max}(G_{max.thr}/G_{max.th})$) curves associated with the data shown in Figure 1. In this empirically-derived expression, the value of $\sqrt{G_{max.thr}}$ ($= 4.79\ \sqrt{(J/m^2)}$) used in Figure 20 is the 'mean-3σ' value given in [17]. The term $G_{max.th}$ is the maximum value of the applied energy release-rate in the fatigue cycle at a value of da/dN of 10^{-10} m/cycle. The values of $G_{max.th}$ appropriate for each curve were obtained by empirically fitting the various curves to a common value of da/dN and G''_{max}, with da/dN being equal to 10^{-10} m/cycle. The values of the terms $G_{max.th}$ so determined are given in Table 4. The normalised da/dN versus G''_{max} curves shown in Figure 20 do indeed reduce the scatter. Such an observation would obviously arise in the near-threshold region, due to the empirical approach used. However, in the regions of the data at faster FCG rates, the scatter between the curves is also much reduced. This arises since

the individual experimental curves shown in Figure 1 all have somewhat similar slopes. Thus, if you force them to go through one point on the plot shown in Figure 20, e.g. at a value of da/dN of 10^{-10} m/cycle, then it will tend to bring all the individual curves into agreement and hence reduce the scatter over the complete range of the curves. Furthermore, the resultant da/dN versus G''_{max} curve is somewhat similar, albeit significantly more conservative, when compared to the worst-case, 'mean-3σ' curve given in [17] which was obtained using the Hartman-Schijve methodology. As may be seen, there is very good agreement between the two different approaches in the near-threshold region but this is to be expected from the empirical-fitting approach used for the da/dN versus G''_{max} curves.

6.2 Delamination growth in IM7/8552 CFRP

To further continue this study, let us next consider delamination growth in the IM7/8552 CFRP tests reported in [6, 17]. The results of twenty-three tests employing G_{max} values tested using 33% to 90% of G_c are shown in Figure 21, where we see significant variability. As shown in Figure 22, this variability is again significantly reduced if da/dN is plotted against G''_{max}. The value of $\sqrt{G_{max.thr}}$ (= 6.28 $\sqrt{(J/m^2)}$) used in Figure 22 is the 'mean-3σ' value given in [17]. The values of $G_{max.th}$ appropriate for each curve were again obtained by empirically fitting the various curves to a common value of da/dN and G''_{max}, with da/dN being equal to 10^{-10} m/cycle, and they are given in Table 5. Figure 22 also reveals that the resultant da/dN versus G''_{max} is somewhat similar, albeit more conservative, to the 'mean-3σ' curve, as commented above with respect to Figure 20.

6.3 Delamination growth in M30SC/DT120 CFRP

Finally, let us consider the delamination growth curves shown in Figures 3 and 4 for the M30SC/DT120 CFRP. Figures 23 and 24 reveal that the variability is significantly reduced if da/dN is plotted against $\Delta\sqrt{G''}$, where $\Delta\sqrt{G''} = \Delta\sqrt{G}(\Delta\sqrt{G_{thr}}/\Delta\sqrt{G_{th}})$. The value of $\Delta\sqrt{G_{thr}}$ (= 3.4 $\sqrt{(J/m^2)}$) used is the 'mean-3σ' value given in [18,19]. The term $\Delta\sqrt{G_{th}}$ is the value of $\Delta\sqrt{G}$ at a value of da/dN of 10^{-10} m/cycle. The values of $\Delta\sqrt{G_{th}}$ appropriate for each curve were obtained by empirically fitting the various curves to a common value of da/dN and $\Delta\sqrt{G''}$, with da/dN being equal to 10^{-10} m/cycle. The values of $\Delta\sqrt{G_{th}}$ used in Figure 23 are given in Table 6 and the values of $\Delta\sqrt{G_{th}}$ used in Figure 24 are given in Table 7. The normalised da/dN versus $\Delta\sqrt{G''}$ curves shown in Figures 23 and 24 do again indeed reduce the scatter. As noted above, such an observation would obviously arise in the near-threshold region, due to the empirically

methodology used. However, in the regions of the data at faster FCG rates, the scatter between the curves is also much reduced in both Figure 23 and 24. Again, this arises since the individual experimental curves shown in Figures 3 and 4 all have very similar slopes. Thus, if you force them to go through one point on the plots shown in Figures 23 and 24, e.g. at a value of da/dN of 10^{-10} m/cycle, then it will tend to bring all the individual curves into agreement and hence reduce the scatter over the complete range of the curves. Furthermore, the resultant da/dN versus $\Delta\sqrt{G''}$ curves are somewhat similar, albeit significantly more conservative, when compared to the worst-case, 'mean-3σ' curve given in [18, 19] which was obtained using the Hartman-Schijve methodology. Finally, as may be seen, there is very good agreement between the two different approaches in the near-threshold regions but this is to be expected from the empirical-fitting approach used for the da/dN versus G''_{max} curves.

7. CONCLUSIONS

If the idea of normalising the experimental delamination curves is to produce an empirically derived master curve, then it would appear that normalising by dividing by $G_R(a)$ does not appear to always achieve this goal, at least not in the important near-threshold region of the FCG rate curves. However, despite the fact that most composite and bonded airframes are designed in accordance with a "no growth" design philosophy there are now instances where disbonding and delamination has been found to grow in operational aircraft. As a result, there is now an interest in allowing for slow delamination growth, and consequently in how to account for growth in the near-threshold region. In the examples studied, we have shown that normalising by dividing by the fatigue threshold appears to reduce the scatter in the delamination growth curves and yields curves that are consistent, albeit significantly more conservative, when compared with the worst-case 'mean-3σ' upper-bound curves obtained using the Hartman-Schijve equation. However, it should be stressed that both approaches are empirical in nature.

ACKNOWLEDGEMENTS

John Michopoulos acknowledges support for this work by the Office of Naval Research (ONR) through the Naval Research Laboratory's core funding. Rhys Jones acknowledges support via an Office of Naval Research (ONR) NICOP Grant N62909-19-1-2011-P00001. The authors would also like to acknowledge the many helpful discussions with Professor Stanzl-Tschegg

at the Institute of Physics and Materials Science, University of Natural Resources and Life Sciences (BOKU) in Vienna, Austria.

REFERENCES

1. MIL-STD-1530D, 2016, Department of Defense Standard Practice; Washington, DC, USA, 2016.
2. Department of Defense Joint Service Specification Guide, Aircraft Structures, JSSG-2006, October 1998.
3. CMH-17-3G, Composite Materials Handbook, Volume 3: Polymer Matrix Composites Materials Useage, Design and Analysis, Published by SAE International, March 2012.
4. Jones R., Peng D., Michopoulos J.G., Kinloch A.J., (2020) Requirements and variability affecting the durability of bonded joints, Materials, 13, 1468.
5. Poursartip A., The characterization of edge delamination growth in laminates under fatigue loading, In: Johnston NJ, editor. Toughened Composites, ASTM STP 937. Philadelphia: American Society for Testing and Materials; 1987. 222–41. Available at https://books.google.com.au/books?id=UCCuywI80PsC&pg=PA222&lpg=PA222&dq=Poursartip+characterization+of+edge+delamination+growth&source=bl&ots=AIaAAO28T6&sig=ACfU3U33mElT9R8K94aZJHHFtOY0pxk7Mg&hl=en&sa=X&ved=2ahUKEwiar5y60tvkAhXDfH0KHUYEBaMQ6AEwBnoECAoQAQ#v=onepage&q=Poursartip%20characterization%20of%20edge%20delamination%20growth&f=false
6. Murri G.B., (2014) Effect of data reduction and fiber-bridging on Mode I delamination characterization of unidirectional composites, Journal of Composite Materials, 48, 2413-2424.
7. Murri G.B. Evaluation of delamination onset and growth characterization methods under mode I fatigue loading. In: ASC 27th technical conference – 15th US-Japan conference on composites, Arlington, TX, October 1–3, 2012.
8. Murri G.B., Evaluation of delamination onset and growth characterization methods under mode I fatigue loading. Langley Research Center, Hampton, Virginia. NASA/TM-2013-217966, 2013.
9. Chen H, Shivakumar K, Abali F., (2006) A comparison of total fatigue life models for composite laminates. Fatigue and Fracture of Engineering Materials and Structures, 1, 31–39.

10. Peng L., Zhang J., Zhao L., Bao R., Yang H, Fei B., (2011) Mode I delamination growth of multidirectional composite laminates under fatigue loading. J. Composite Materials, 45, 1077–1090.
11. Yao L., Sun Y., Guo L., Zhao M., Jia L., Alderliesten R.C., et al., (2017) A modified Paris relation for fatigue delamination with fibre bridging in composite laminates, Composite Structures, 176, 556–564.
12. Yao L., Sun Y., Guo L., Lyu X., Zhao M., Jia L., Alderliesten R.C., Benedictus R., (2018) Mode I fatigue delamination growth with fibre bridging in multidirectional composite laminates, Engineering Fracture Mechanics, 189, 221–231.
13. Rocha A.V.M,, Akhavan-Safar A., Carbas R., Marques E.A.S., Goyal R. , El-Zein M., da Silva L.F.M., (2020) Paris law relations for an epoxy-based adhesive. Proc. IMechE. Part L: J Materials: Design and Applications, 234, 291–299.
14. Al-Khudairi O., Hadavinia H., Waggott A., Lewis E., Little C., (2015) Characterising mode I/mode II fatigue delamination growth in unidirectional fibre reinforced polymer laminates, Materials and Design, 66, 93–102.
15. Gong Y., Zhao L., Zhang J., Hu N., Zhang C., (2019) An insight into three approaches for determining fatigue delamination resistance in DCB tests on composite laminates, Composites Part B, 176, 107206.
16. Gong Y., Zhao L., Zhang J., Hu N., (2018) A novel model for determining the fatigue delamination resistance in composite laminates from a viewpoint of energy, Composites Science and Technology, 167, 489–496.
17. Jones R., Kinloch A.J., Michopoulos J.G., Brunner A.J., Phan N., (2017) Delamination growth in polymer-matrix fibre composites and the use of fracture mechanics data for material characterisation and life prediction, Composite Structures, 180, 316-333.
18. Yao L., Alderliesten R., Jones R., Kinloch A.J., (2018) Delamination fatigue growth in polymer-matrix fibre composites: A methodology for determining the design and lifing allowables, Composite Structures, 96, 8-20.
19. Kinloch A.J., Jones R., (2020) A way forward for industry to determine valid cyclic-fatigue relationships for polymer-matrix fibre composites, Proceedings 1st Virtual European Conference on Fracture (VECF1), June 29, 2020. Procedia Structural Integrity, to be published.
20. Jones R, Pitt S., Brunner A.J., Hui D., (2013) Fatigue crack growth in nano-composites, Composite Structures, 99, 375-379.

21. Jones R., Pitt S., Brunner A.J., Hui D., (2012) Application of the Hartman-Schijve equation to represent Mode I and Mode II fatigue delamination growth in composites, Composite Structures, 94, 1343-1351.
22. Jones R., Stelzer S., Brunner A.J., (2014) Mode I, II and mixed Mode I/II delamination growth in composites, Composite Structures, 110, 317-324.
23. Hartman A. and Schijve J., (1970) The effects of environment and load frequency on the crack propagation law for macro fatigue crack growth in aluminium alloys, Engineering Fracture Mechanics, 1, 615-631.
24. Schwalbe K.H., (2010) On the Beauty of Analytical Models for Fatigue Crack Propagation and Fracture-A Personal Historical Review, J. ASTM Intl., 7, 3-73.
25. Ramsamooj D.V. (2003) Analytical prediction of short to long fatigue crack growth rate using small- and large-scale yielding fracture mechanics, International Journal of Fatigue, 25, 923-33.
26. McEvily A.J., Eifler D., Macherauch E., (1991) An analysis of the growth of short fatigue cracks, Fatigue and Fracture of Engineering Materials and Structures, 40, 571-84.
27. Endo M., McEvily A.J., (2007) Prediction of the behaviour of small fatigue cracks, Mater. Sci. Eng. A, 468-470, 51-8.
28. Ishihara S., Yoshifuji S., McEvily A.J., Kawamoto M., Sawai M, Takata M., (2010) Study of the fatigue lifetimes and crack propagation behaviour of a high speed steel as a function of the R value, Fatigue and Fracture of Engineering Materials and Structures, 33, 294-302.
29. Wang K., Wang F., Cui W., Hayat T., Ahmad B., (2014) Prediction of short fatigue crack growth of Ti-6Al-4V, Fatigue and Fracture of Engineering Materials and Structures, 37, 1075-1086.
30. Jones R., Peng D., McMillan A.J., (2018) Crack growth from naturally occurring material discontinuities, Chapter 5, pp. 129-190, Aircraft Sustainment and Repair, Edited by Jones R., N. Matthews, AA. Baker and V. Champagne Jr., Butterworth-Heinemann Press, ISBN 9780081005408.
31. Jones R., Molent L., Barter S., (2013) Calculating crack growth from small discontinuities in 7050-T7451 under combat aircraft spectra, International Journal of Fatigue, 55, 178-182.

32. Tamboli D., Barter S., Jones R., (2018) On the growth of cracks from etch pits and the scatter associated with them under a miniTWIST spectrum, International Journal of Fatigue, 109, 10-16.
33. Main B., Evans R., Walker, K. Yu X., Molent L., (2019) Lessons from a Fatigue Prediction Challenge for an Aircraft Wing Shear Tie Post, International Journal of Fatigue, 123, 53-65.
34. Tan J.L., Chen B.K., (2015) Prediction of fatigue life in aluminium alloy (AA7050-T7451) structures in the presence of multiple artificial short cracks, Theoretical and Applied Fracture Mechanics, 78, 1-7.
35. Jones R., Singh Raman R.K., McMillan A.J., (2018) Crack growth: Does microstructure play a role?, Engineering Fracture Mechanics, 187, 190-210.
36. Lo M., Jones R., Bowler A., Dorman M., Edwards D., (2017) Crack growth at fastener holes containing intergranular cracking, Fatigue and Fracture of Engineering Materials and Structures, 40, 1664-1675.
37. Jones R., Peng D., Singh Raman R.K., Huang P., Tamboli D., Matthews N., (2015) On the growth of fatigue cracks from corrosion pits and manufacturing defects under variable amplitude loading, JOM, 67, 1385-1391.
38. Zhang Y., Zheng K., Heng J., Zhu J., (2019) Corrosion-Fatigue Evaluation of Uncoated Weathering Steel Bridges, Appl. Sci., 9, 3461.
39. Ali K., Peng D., Jones R., Singh R. R. K., Zhao X.L., McMillan A.J., Berto F., (2017) Crack growth in a naturally corroded bridge steel, Fatigue and Fracture of Engineering Materials and Structures, 40, 1117-1127.
40. Godefroid L.B., Moreira L.P., Vilela T.C.G., Faria G.L., Candido L.C., Pinto E.S., (2019) Effect of chemical composition and microstructure on the fatigue crack growth resistance of pearlitic steels for railroad application, International Journal of Fatigue, 120, 241-253.
41. Brunner, A.J., Stelzer, S., Pinter, G., Terrasi, G.P., (2016) Cyclic fatigue delamination of carbon fiber-reinforced polymer-matrix composites: Data analysis and design considerations, International Journal of Fatigue, 83, 293-299.
42. Chocron, T., Banks-Sills, L., (2019) Nearly Mode I fracture toughness and fatigue delamination propagation in a multidirectional laminate fabricated by a wet-layup, Physical Mesomechanics, 22, 107-140.

43. Simon, L., Banks-Sills, L., Fourman, V., (2017) Mode I delamination propagation and R-ratio effects in woven composite DCB specimens for a multi-directional layup, International Journal of Fatigue, 96, 237-251.
44. Jones R. Kinloch A.J., Hu W., (2016) Cyclic-fatigue crack growth in composite and adhesively-bonded structures: the FAA slow crack growth approach to certification and the problem of similitude, International Journal of Fatigue, 88, 10-18.
45. Jones R., Hu W., Kinloch A.J., (2015) A convenient way to represent fatigue crack growth in structural adhesives, Fatigue and Fracture of Engineering Materials and Structures, 38, 379-391.
46. Jones R., Kinloch A.J., Michopoulos J.G., Peng D., (2020) A means for industry to determine the economic life of bonded joints under representative operation flight loads Proceedings 1st Virtual European Conference on Fracture (VECF1), June 29, 2020. Procedia Structural Integrity, to be published.
47. Clerc, G., Brunner, A.J., Niemz, P., Van de Kuilen, J.W.G. (2020) Feasibility study on Hartman-Schijve data analysis for Mode II fatigue fracture of adhesively bonded wood joints, International Journal of Fracture, 221, 123-140.
48. Cano AJ., Salazar A., Rodríguez J., (2018) Evaluation of different crack driving forces for describing the fatigue crack growth behaviour of PET-G, International Journal of Fatigue, 107, 27-32.
49. Wang, J., Zuo, J., Sun, Y., Wen J., (2020) The effects of thermal treatments on the fatigue crack growth of Beishan granite: an in situ observation study, Bulletin of Engineering Geology and the Environment, Springer Press, https://doi.org/10.1007/s10064-020-01966-w.
50. Jones R., Singh Raman R.K., Iliopoulos A.P., Michopoulos J.G., Phan N., Peng D., (2019) Additively manufactured Ti-6Al-4V replacement parts for military aircraft, International Journal of Fatigue, 124, 227-235.
51. Jones R., Michopoulos J.G., Iliopoulos AP., Singh Raman R.K., Phan N., Nguyen T., (2018) Representing Crack Growth In Additively Manufactured TI-6AL-4V, International Journal of Fatigue, 111, 610-622.
52. Iliopoulos A.P., Jones R., Michopoulos J.G., Phan N.N., Singh Raman, R.K., (2019) Crack growth in a range of additively manufactured aerospace structural materials, Special Issue, Civil and Military Airworthiness: Recent Developments and Challenges, Aerospace, doi:10.3390/aerospace5040118

53. Kundu S., Jones R., Peng D., Matthews N., Alankar A., Singh Raman, R.K., Huang P., (2020) Review of Requirements for the Durability and Damage Tolerance Certification of Additively Manufactured Aircraft Structural Parts and AM Repairs, Materials 2020, 13, 1341.
54. Jones R., Matthews N., Peng D., Phan N., Nguyen T.T., (2019) Damage Tolerant Assessment Of Additively Manufactured Replacement Parts, Proceedings 13th International Conference on the Mechanical Behaviour of Materials (ICM13), 11th - 14th June 2019, Melbourne, Australia.
55. Jones R., Matthews N., Peng D., Phan N. and Nguyen T., Applications of SPD to enhance the structural integrity of corroded airframes, Chapter 16, pp. 863-906, Aircraft Sustainment and Repair, Edited by R. Jones, N. Matthews, AA. Baker and V. Champagne Jr., Elsevier Butterworth-Heinemann Press, 2018, ISBN 9780081005408.
56. Rans C, Alderliesten R.C., Benedictus R., (2011) Misinterpreting the results: how similitude can improve our understanding of fatigue delamination growth, Composites Science Technology, 71, 230–238.
57. Yao L., Sun Y., Alderliesten R.C., Benedictus R., Zhao M., (2017) Fibre bridging effect on the Paris relation for mode I fatigue delamination growth in composites with consideration of interface configuration, Composite Structures, 159, 471-478.
58. Yao L., Sun Y., Zhao M., Alderliesten R.C., Benedictus R., (2017) Stress ratio dependence of fibre bridging significance in mode I fatigue delamination growth of composite laminates, Composites A, 95, 65-74.
59. Yao L., Sun Y., Guo L., Alderliesten R.C., Benedictus R., Zhao M., Jia, L., (2017) Fibre bridging effect on the Paris relation on mode I fatigue delamination in composite laminates with different thicknesses, International Journal of Fatigue, 103, 196-206.
60. Sun Y., Yao L., Alderliesten R.C., Benedictus R., (2016) Mode I quasi-static delamination growth in multidirectional composite laminates with different thicknesses. Proceedings 31st Technical Conference, American Society for Composites, 1115-1125.
61. Rans, C.D., Atkinson, J., Li, C., (2015) On the onset of the asymptotic stable fracture region in the Mode II fatigue delamination growth behaviour of composites, Journal of Composite Materials, 49, 685-697.
62. Yao L., Cui H., Sun Y., Guo L., Chen X., Zhao M., Alderliesten R.C., (2018) Fibre-bridged fatigue delamination in multidirectional composite laminates, Composites Part A, 115, 175-186.

63. Schönbauer B., Perlega A., Karr U.P., D. Gandy D., Stanzl-Tschegg S.E., (2015) Pit-to-crack transition under cyclic loading in 12% Cr steam turbine blade steel, International Journal of Fatigue, 76, 19-32.
64. Jones R., Molent L., Barter S., (2013) Calculating crack growth from small discontinuities in 7050-T7451 under combat aircraft spectra, International Journal of Fatigue, 55, 178-182.
65. Kujawski D., (2001) Enhanced model of partial crack closure for correlation of R-ratio effects in aluminum alloys, International Journal of Fatigue, 23, 95-102.
66. Kujawski D., (2002) Utilization of partial crack closure for fatigue crack growth modeling, Engineering Fracture Mechanics, 69, 1315–1324.
67. Forman, R.G., Shivakumar V., Cardinal J.W., Williams L.C. and McKeighan P.C., Fatigue crack growth data base for damage tolerance analysis, DOT/FAA/AR-05/15, Aug 2005.
68. Martelo D.F., Mateo A., Chapetti M.D., (2015) Crack closure and fatigue crack growth near-threshold of a metastable austenitic stainless steel, International Journal of Fatigue, 77, 64–77.
69. Kim S., Burns J.T., Gangloff R.P., (2009) Fatigue crack formation and growth from localized corrosion in Al-Zn-Mg-Cu, Engineering Fracture Mechanics, 76, 651-667.
70. Jones R., Lo M., Peng D., Bowler A., Dorman M., Janardhana M. and Iyyer N. S., (2014) A study into the interaction of intergranular cracking and cracking form corrosion pits at fastener holes, Meccanica, 50, 517-532.
71. Hu X., Xue Z., Ren T.T., Jiang Y., Dong C.L., Liu F., (2020) On the fatigue crack growth behaviour of selective laser melting fabricated Inconel 625: Effects of build orientation and stress ratio, Fatigue and Fracture of Engineering Materials and Structures, 43, 771–787.

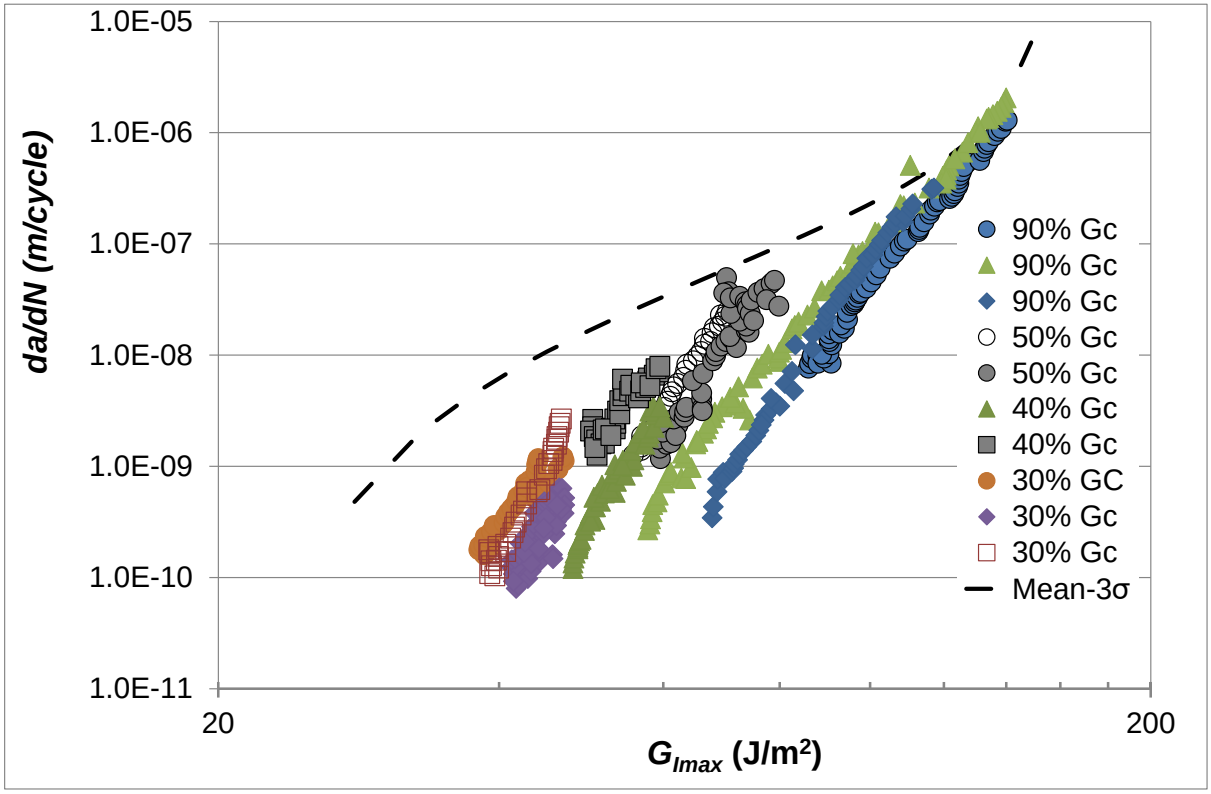

Figure 1. The delamination growth curves for IM7/977-3 CFRP using DCB specimens tested at 90, 50, 40 and 30% of G_c, from [6].

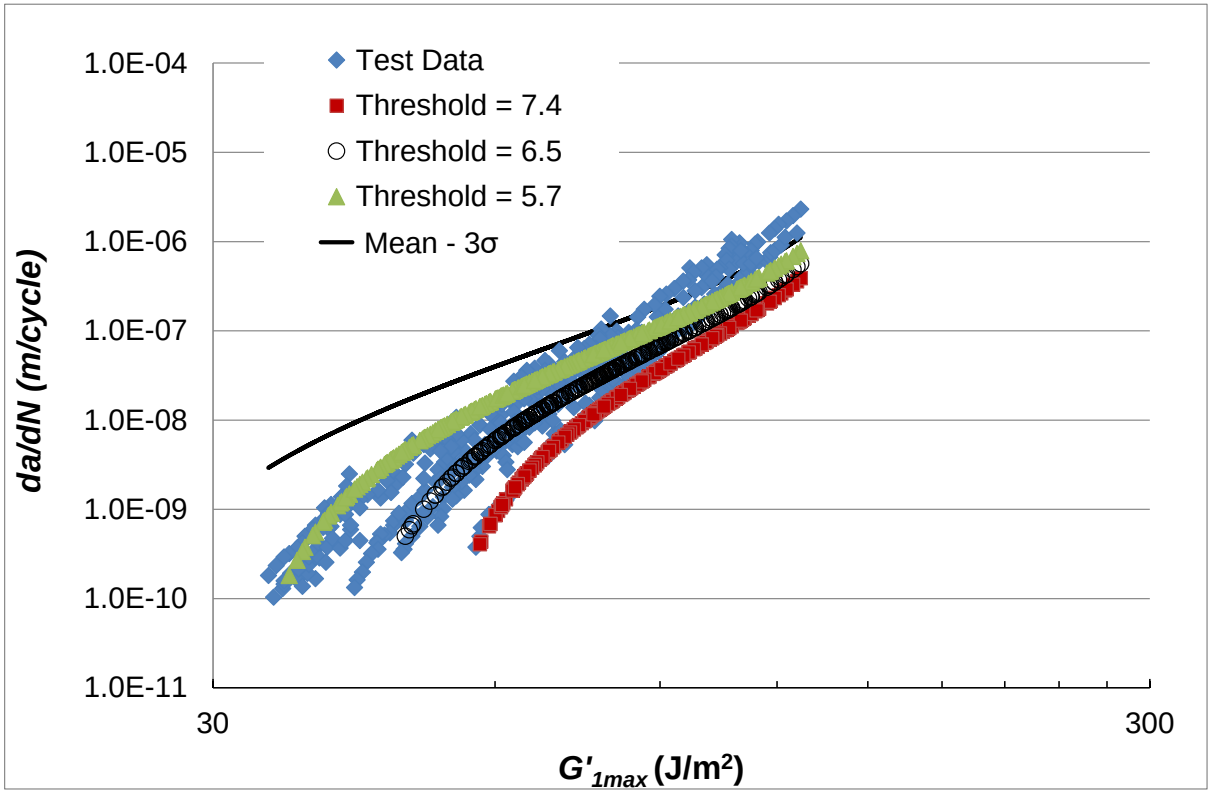

Figure 2. The normalised delamination growth curves for IM7/977-3 CFRP, from [6], and the upper-bound ('mean - 3σ') curve from the Hartman-Schijve methodology given in [17].

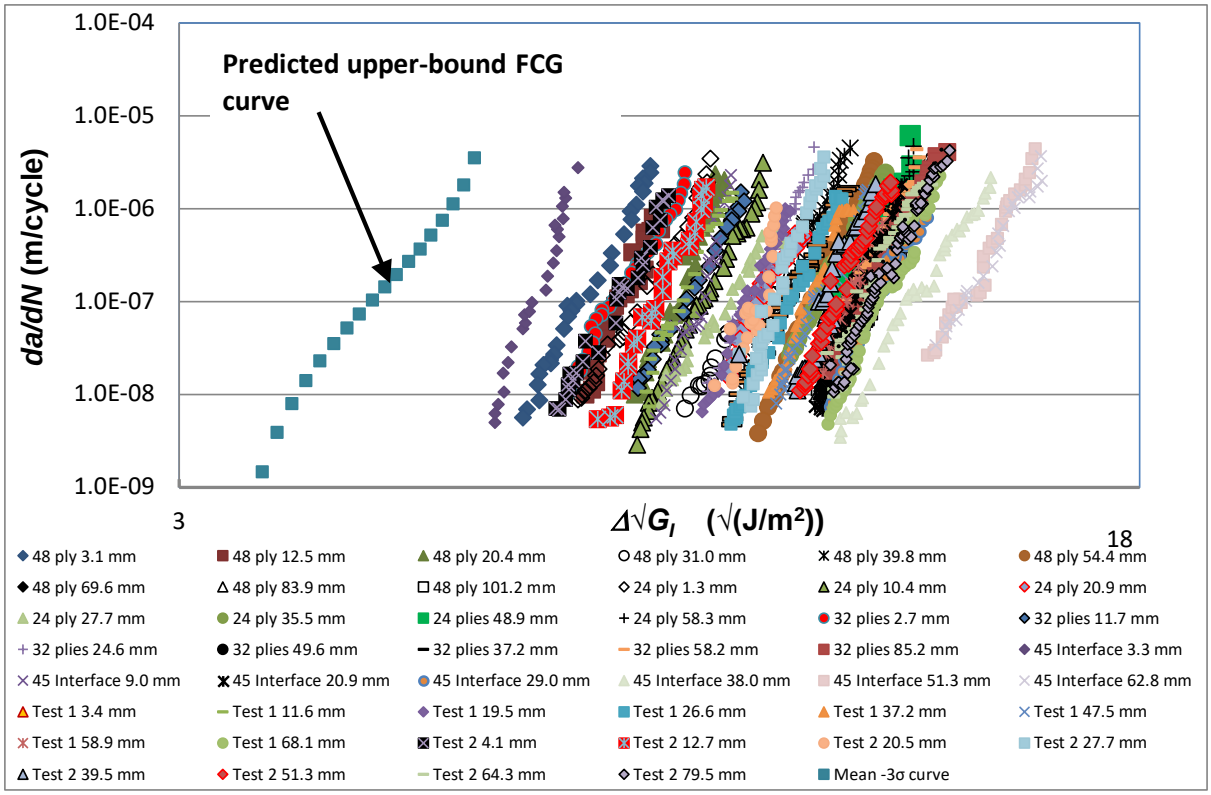

Figure 3. The delamination growth curves for M30SC/DT120 CFRP and the upper-bound ('mean - 3σ') curve given in [18]. (Values are given in the legend for the pre-crack extension length, a_p - a_o, prior to the start of measurements from a DCB fatigue test.)

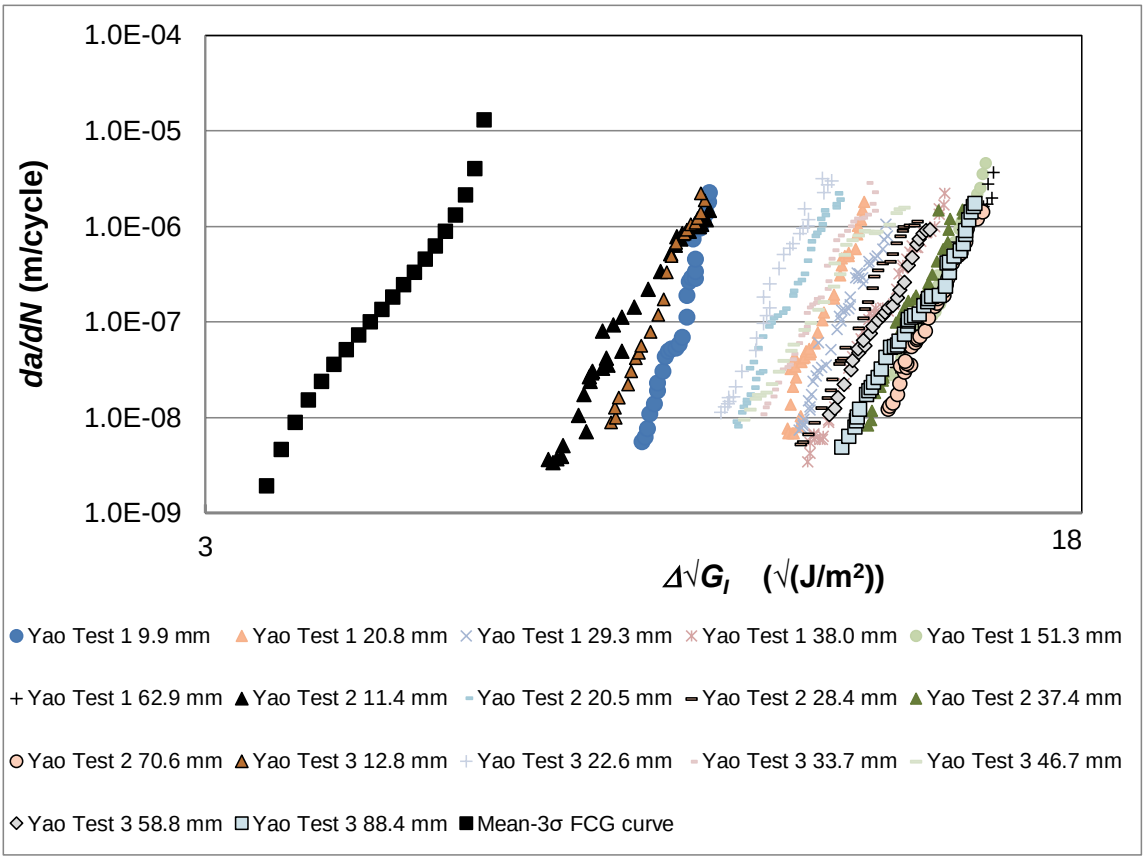

Figure 4. The delamination growth curves for M30SC/DT120 CFRP, from [62], and the upper-bound ('mean - 3σ') curve given in [18]. (Results from three replicate tests are shown. Values are given in the legend for the pre-crack extension length, a_p - a_o, prior to the start of measurements from a DCB fatigue test.)

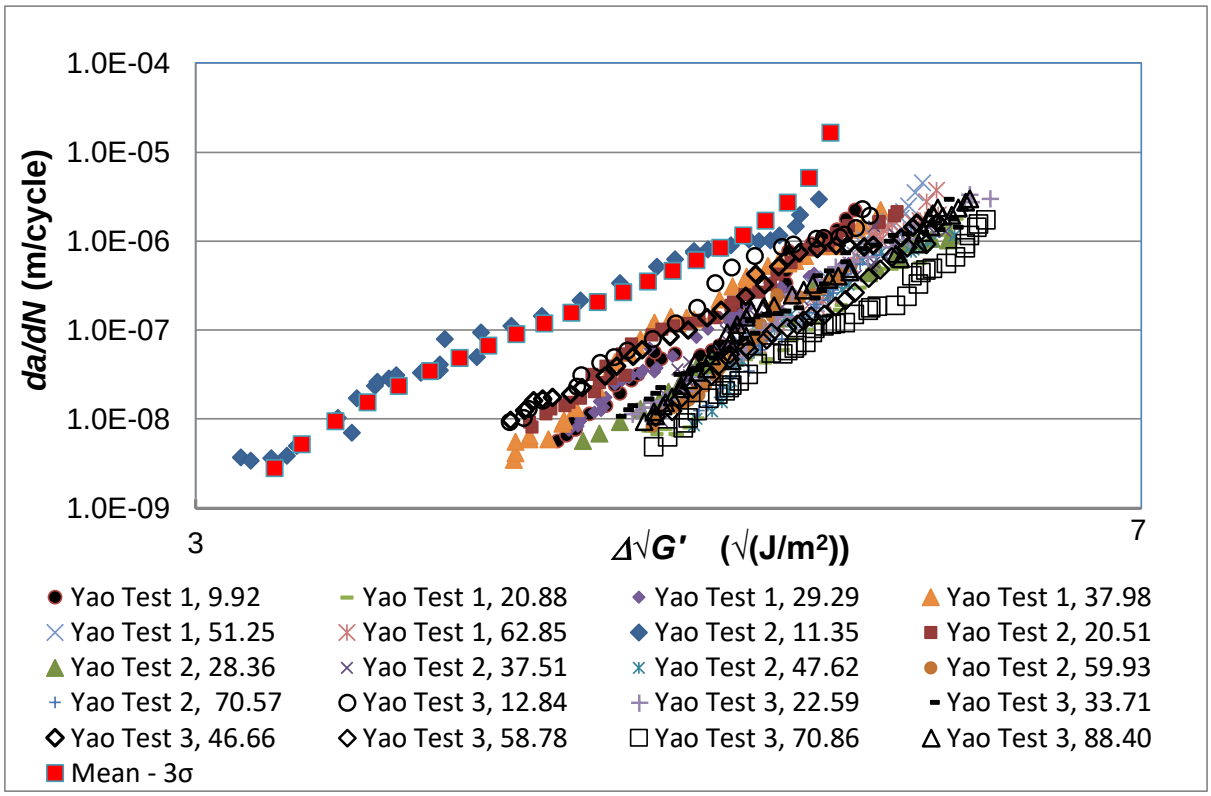

Figure 5. The normalised delamination growth curves for M30SC/DT120 CFRP [62] for the results shown in Figure 4. The upper-bound ('mean - 3σ') curve from the Hartman-Schijve methodology is taken from [18].

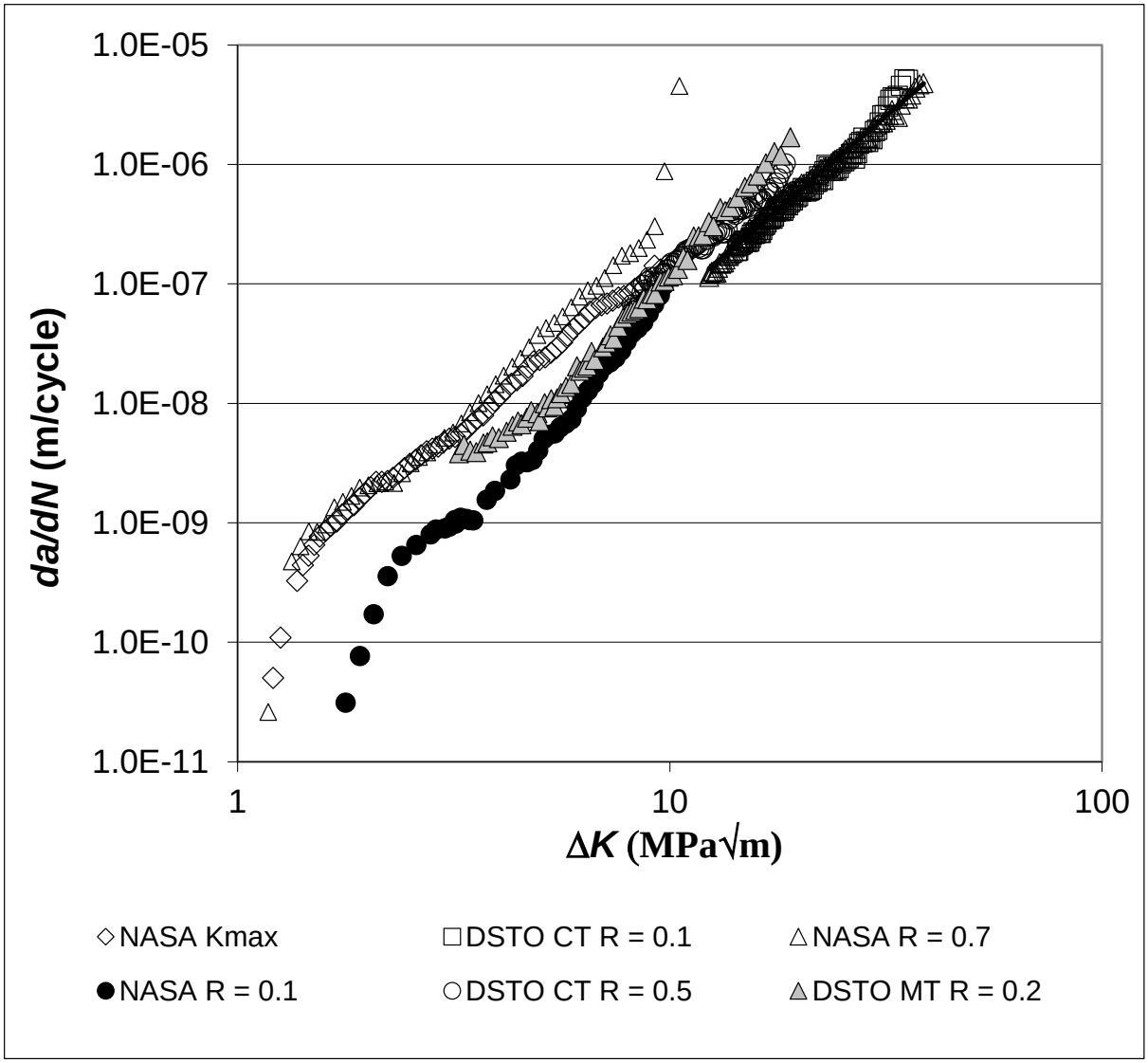

Figure 6. Various aluminium-alloy 7050-T7451 *da*/*dN* versus Δ*K* curves reported in [64].

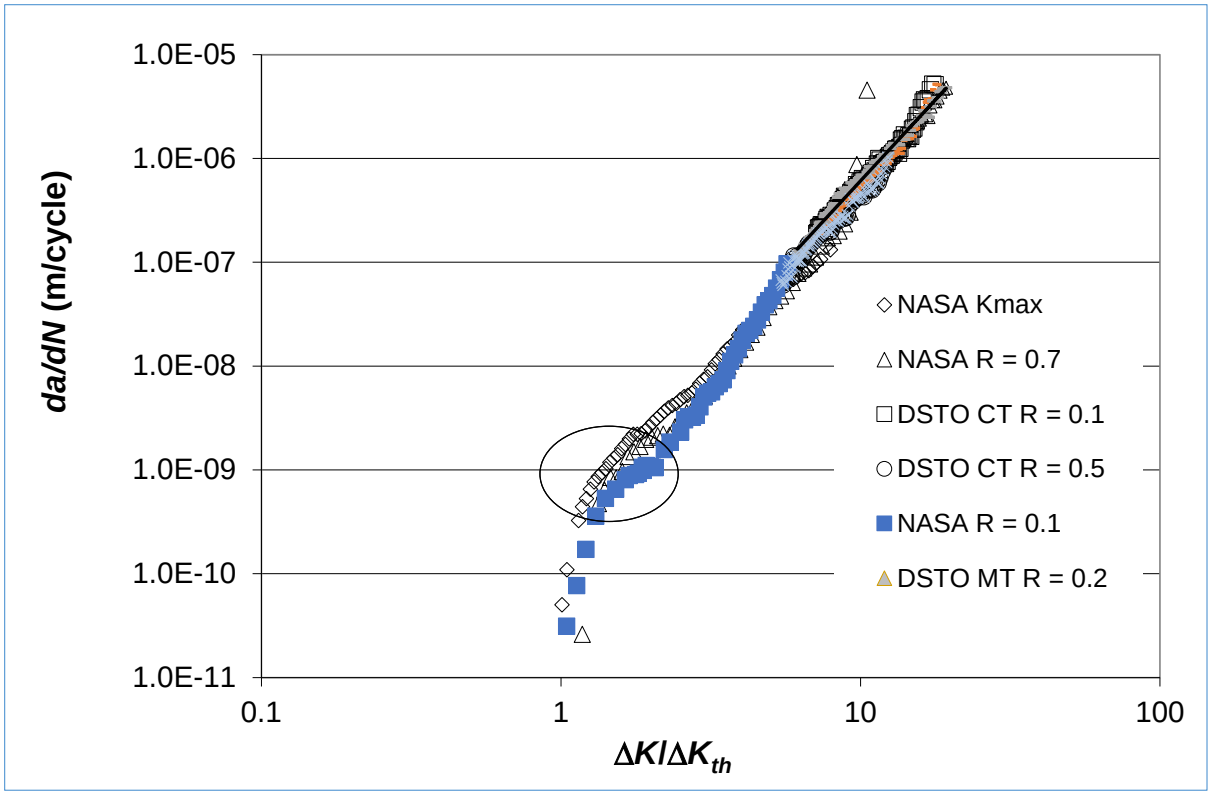

Figure 7. Various *da*/*dN* versus $\Delta K/\Delta K_{th}$ curves for aluminium-alloy 7050-T7451.

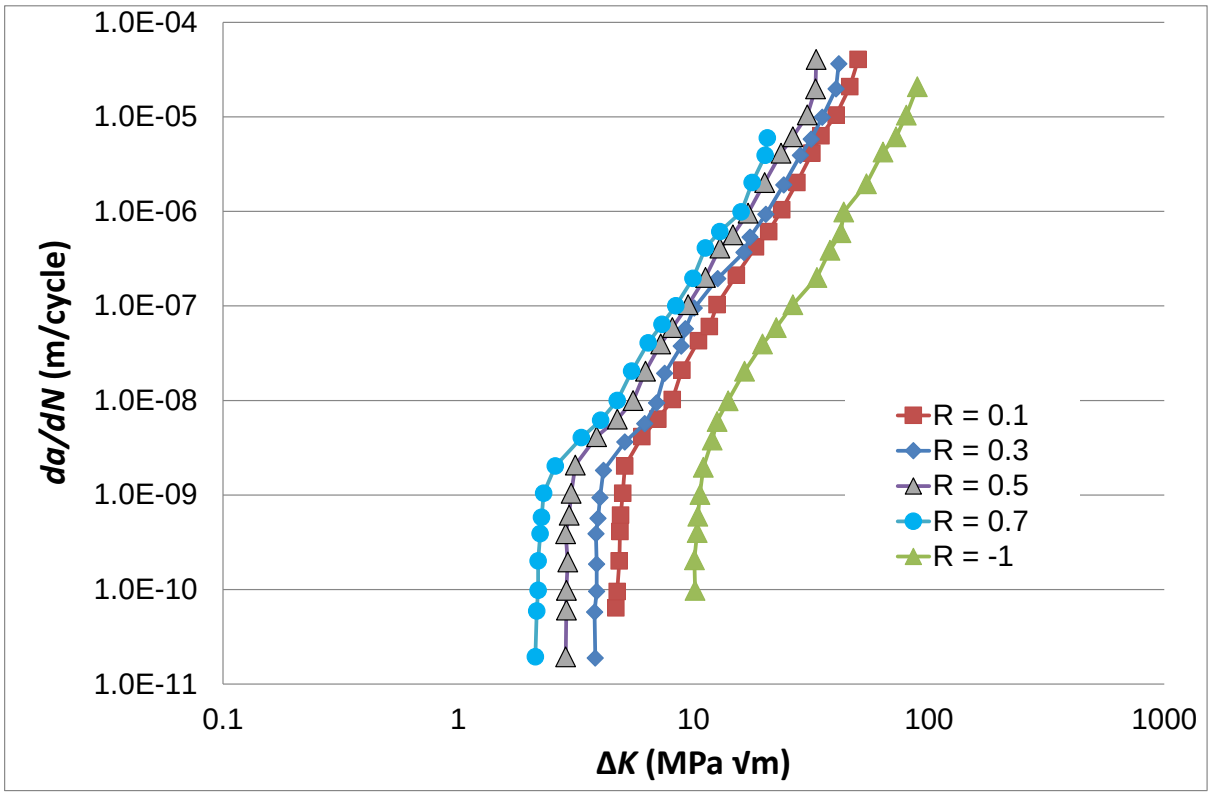

Figure 8. Various *da*/*dN* versus ΔK for aluminium-alloy 2324-T39 presented in [65].

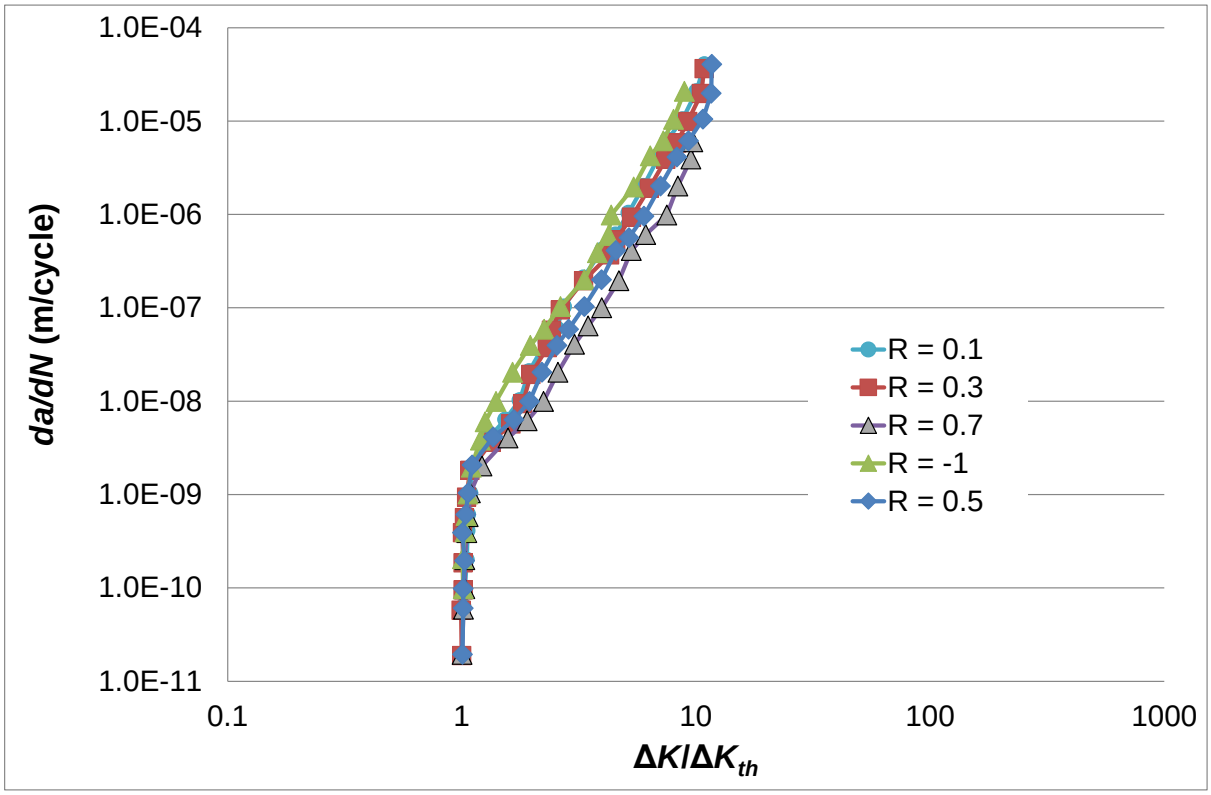

Figure 9. Various da/dN versus $\Delta K/\Delta K_{th}$ for aluminium-alloy 2324-T39 presented in [65] replotted.

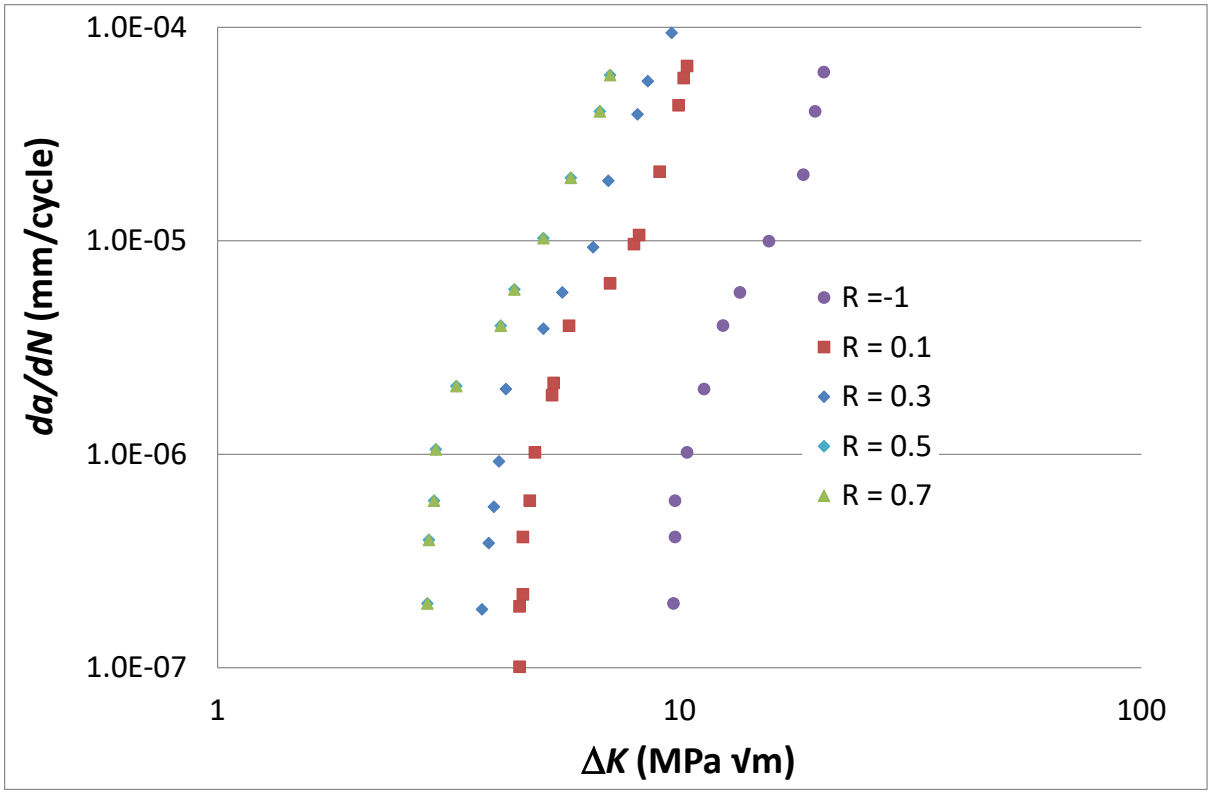

Figure 10. Various *da*/*dN* versus Δ*K* data for aluminium-alloy 6013-T651 presented in [66].

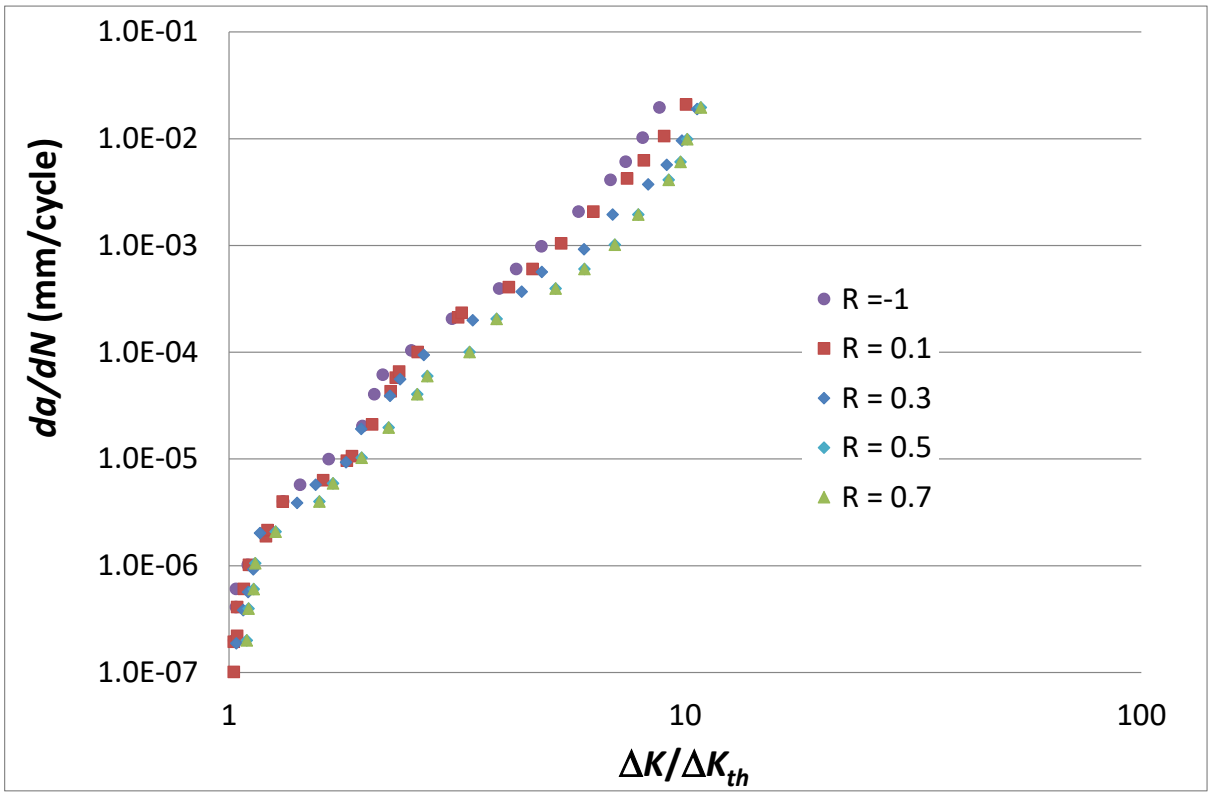

Figure 11. Various d*a*/d*N* versus $\Delta K/\Delta K_{th}$ curves for aluminium-alloy 6013-T651 presented in [66].

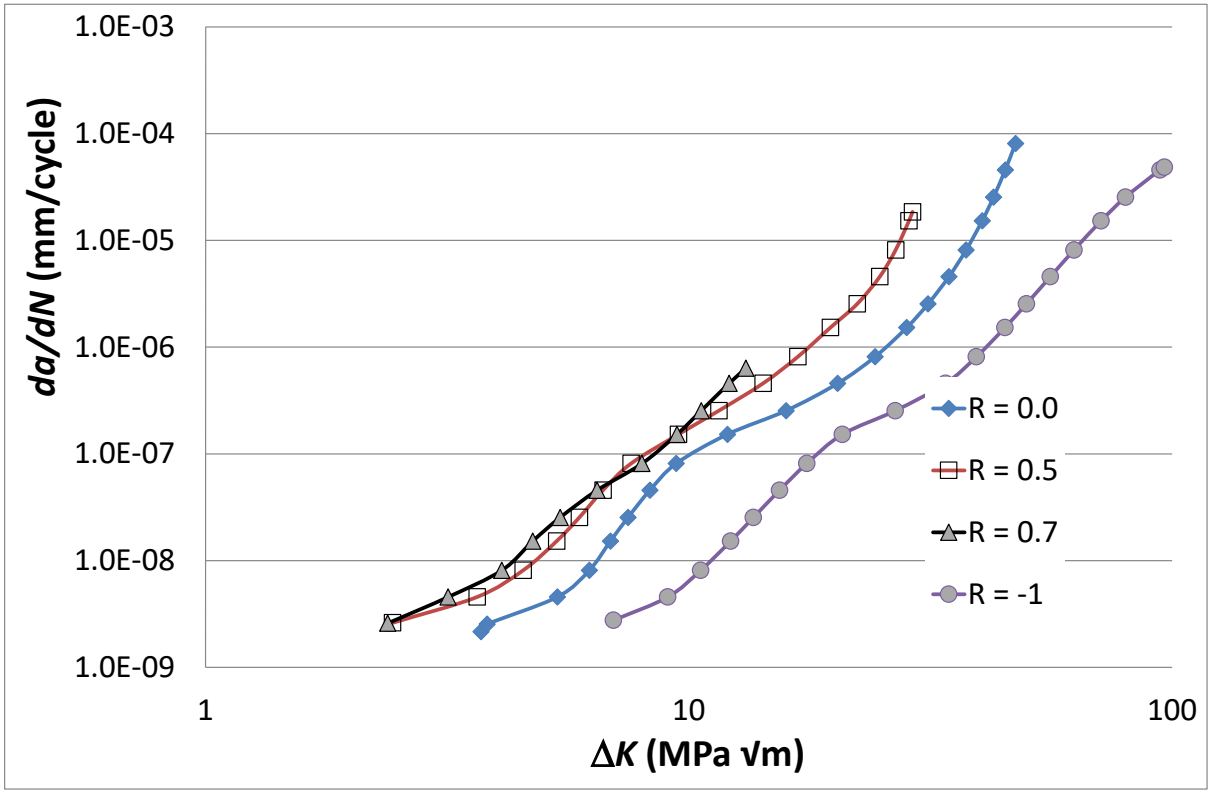

Figure 12. Various *da*/*dN* versus Δ*K* curves for aluminium-alloy 2024-T3, from [67].

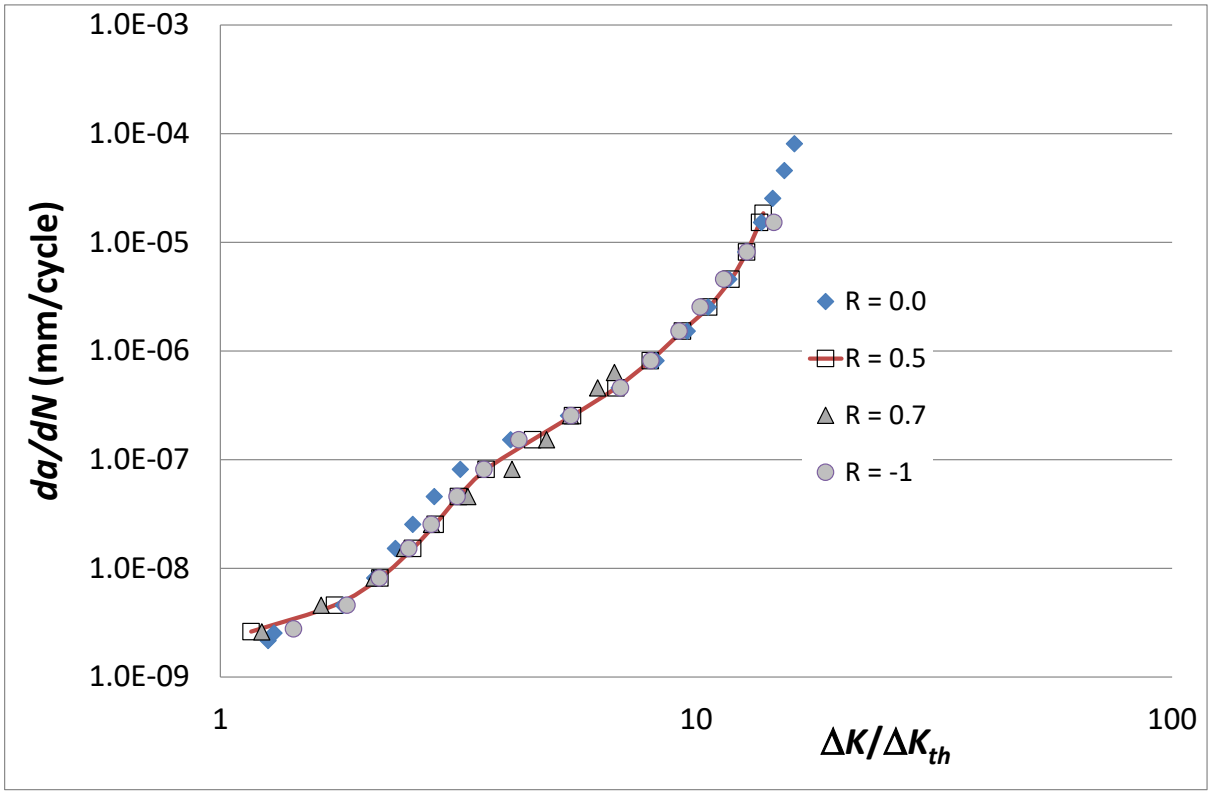

Figure 13. Various *da*/*dN* versus $\Delta K/\Delta K_{th}$ curves for aluminium-alloy 2024-T3, from [67].

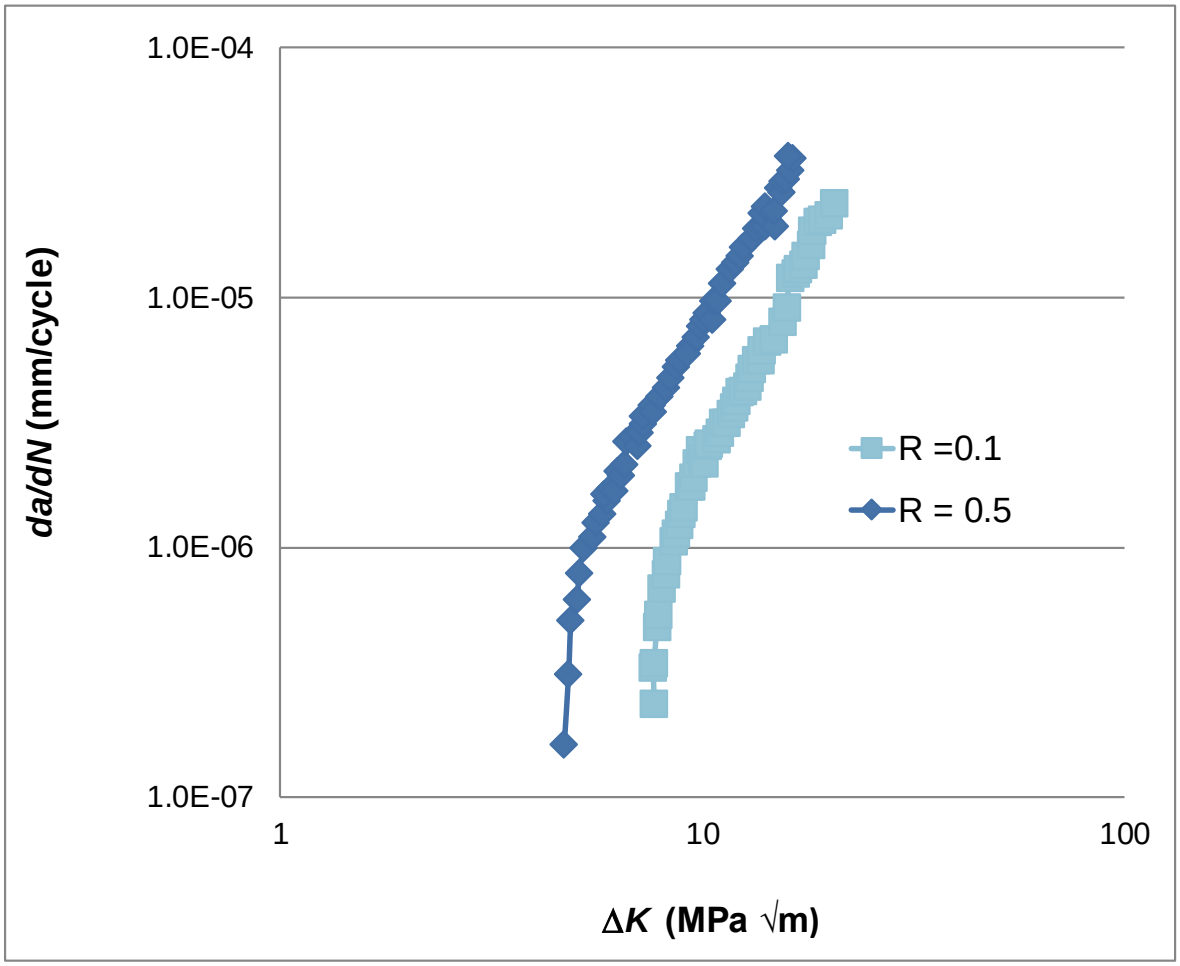

Figure 14. Various *da*/*dN* versus Δ*K* for a cold-rolled metastable austenitic stainless steel tested at *R* = 0.1 and *R* = 0.5, from [68].

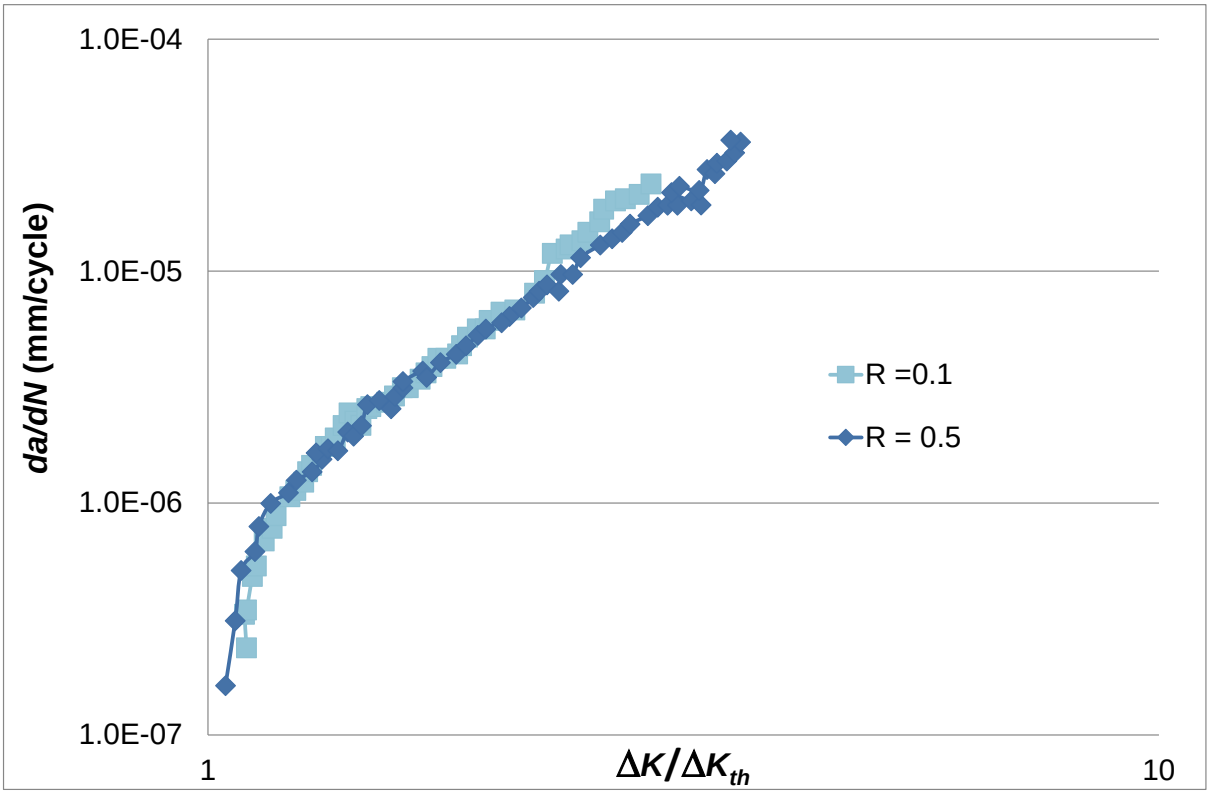

Figure 15. Various da/dN versus $\Delta K/\Delta K_{th}$ curves for a cold-rolled metastable austenitic stainless steel tested at R = 0.1 and R = 0.5, from [68].

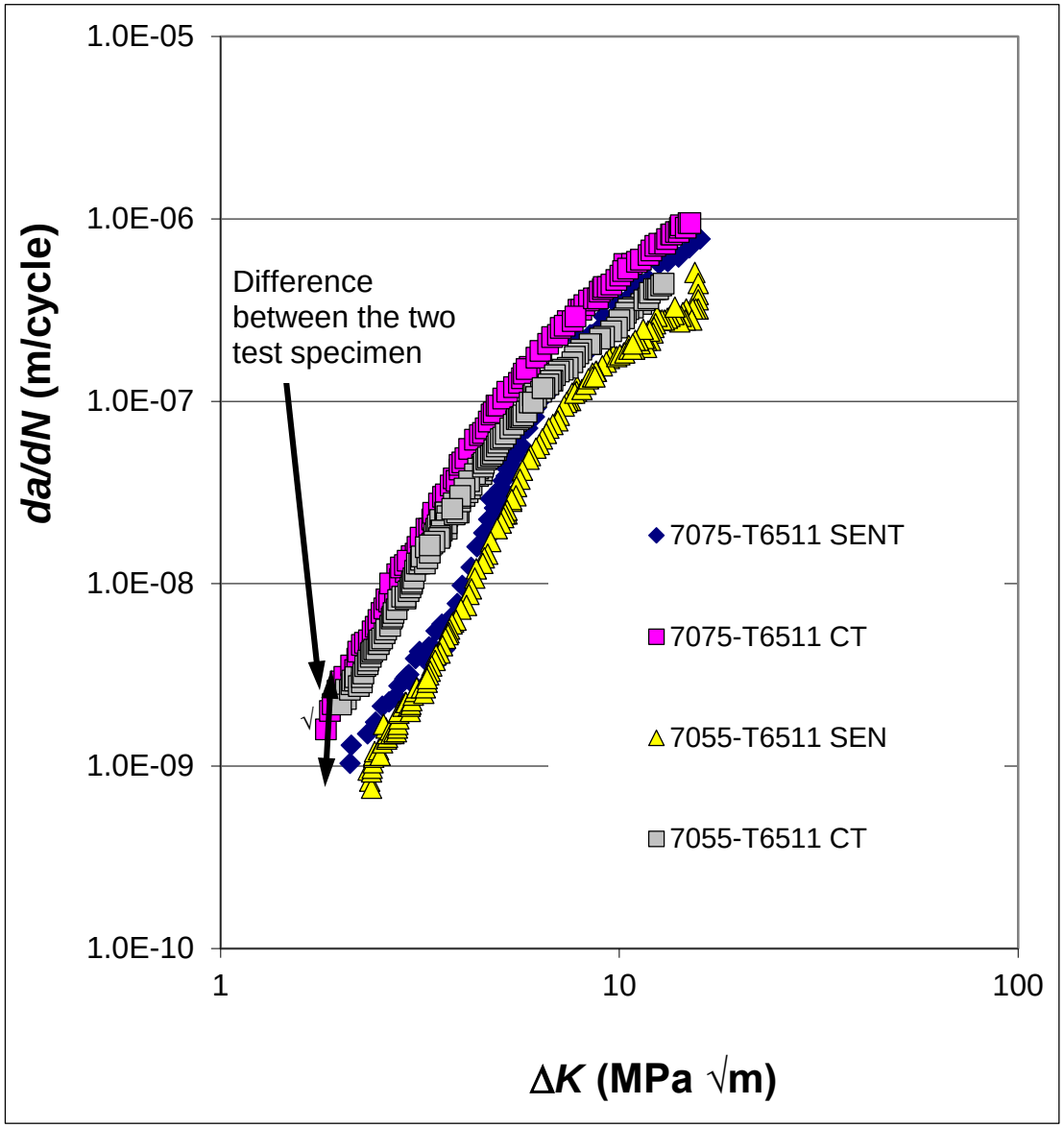

Figure 16. Various *da*/*dN* versus Δ*K* data presented in [69] for aluminium-alloy 7075-T6511.

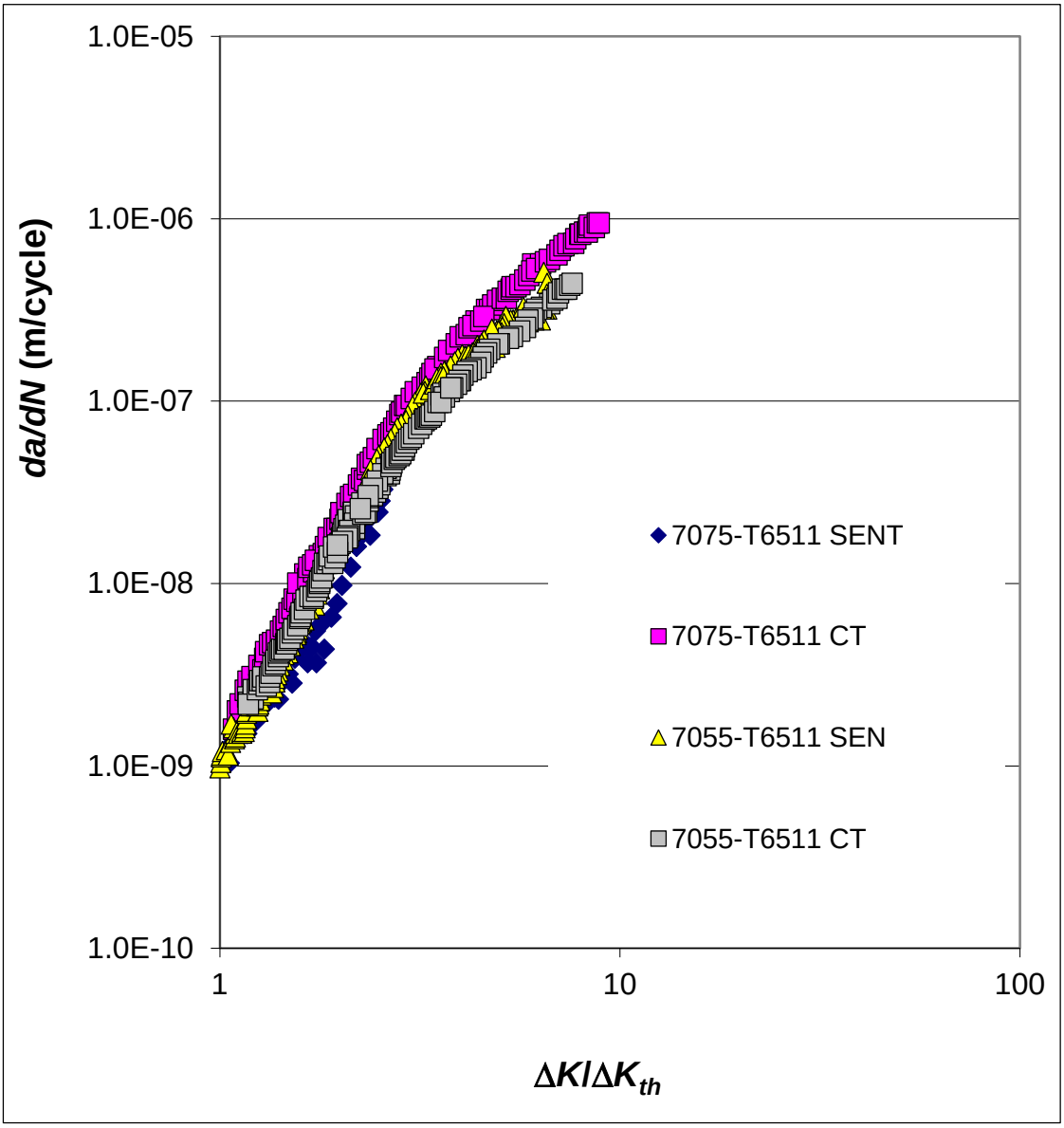

Figure 17. The test data presented in [69] replotted as da/dN versus $\Delta K/\Delta K_{th}$ curves [70].

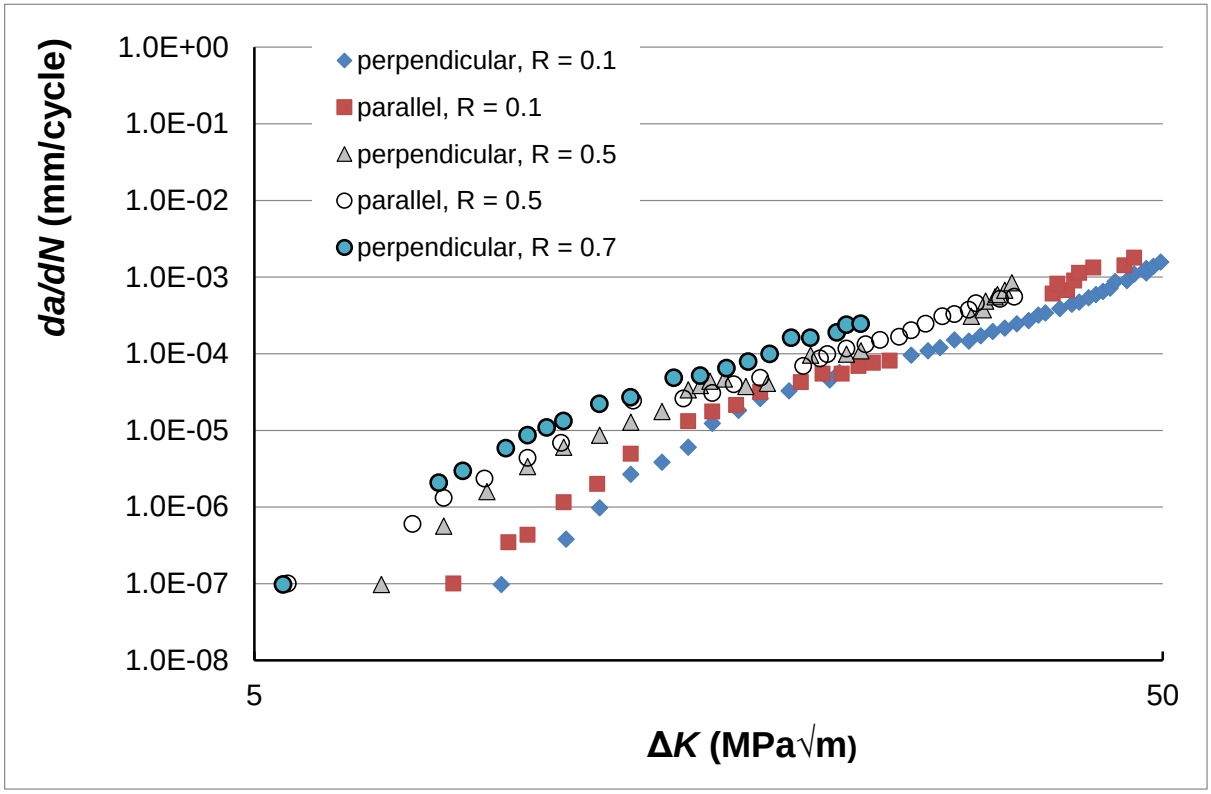

Figure 18. Various *da*/*dN* versus Δ*K* curves presented in [71].

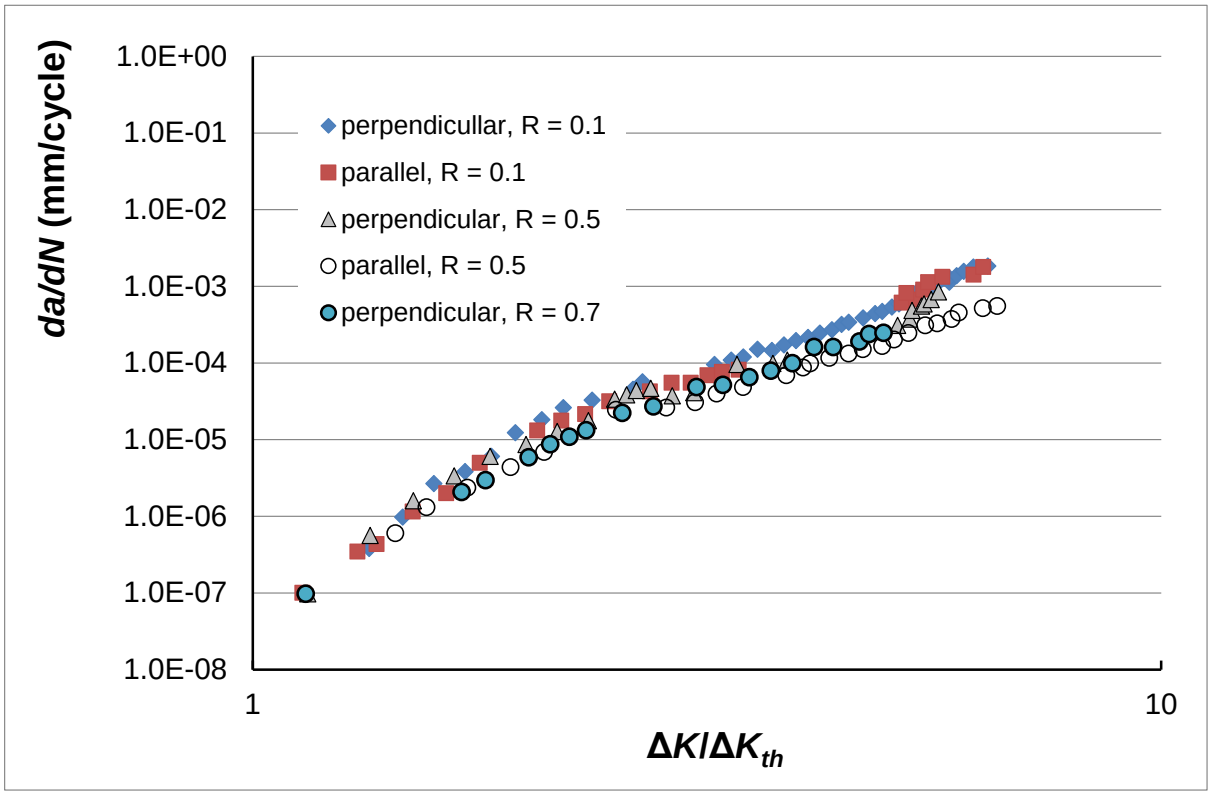

Figure 19. The test data presented in [71] replotted as *da*/*dN* versus $\Delta K/\Delta K_{th}$ curves.

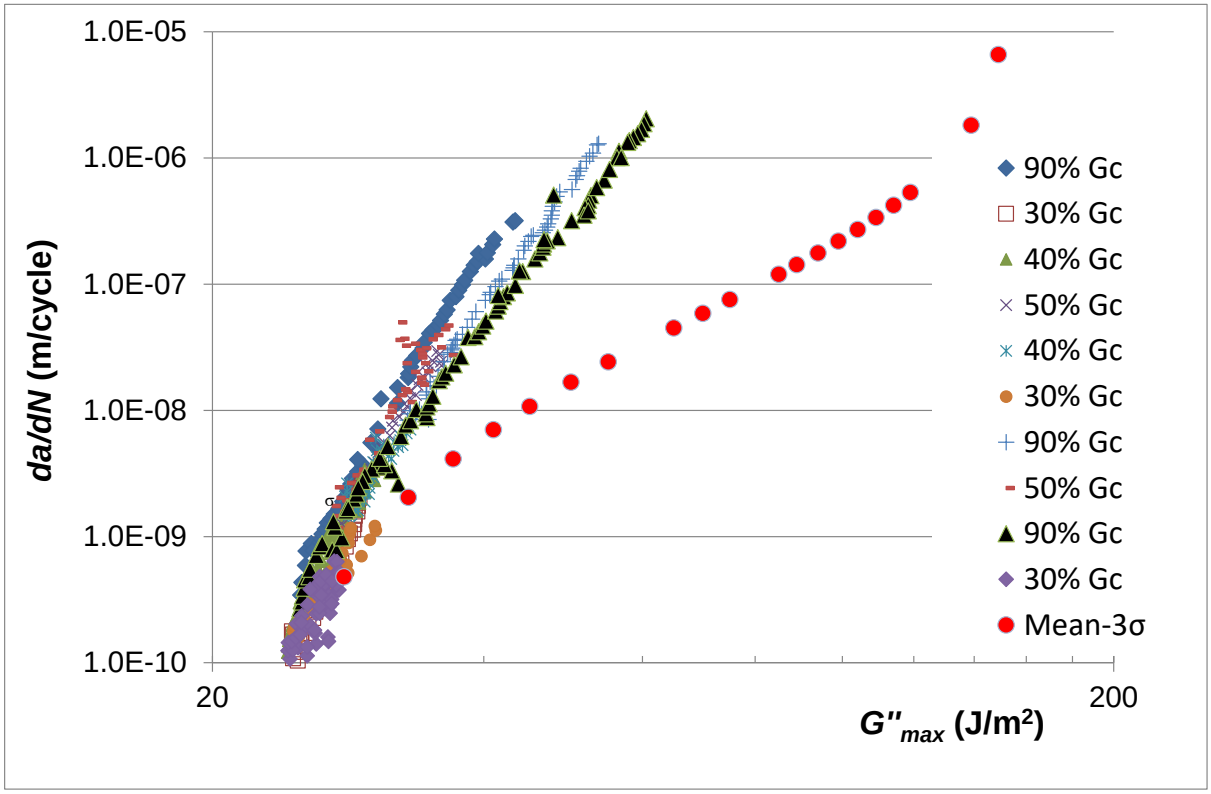

Figure 20. Comparison of the various scaled *da*/*dN* versus G''_{max} plots for the IM7/977-3 CFRP tests analysed in [17].

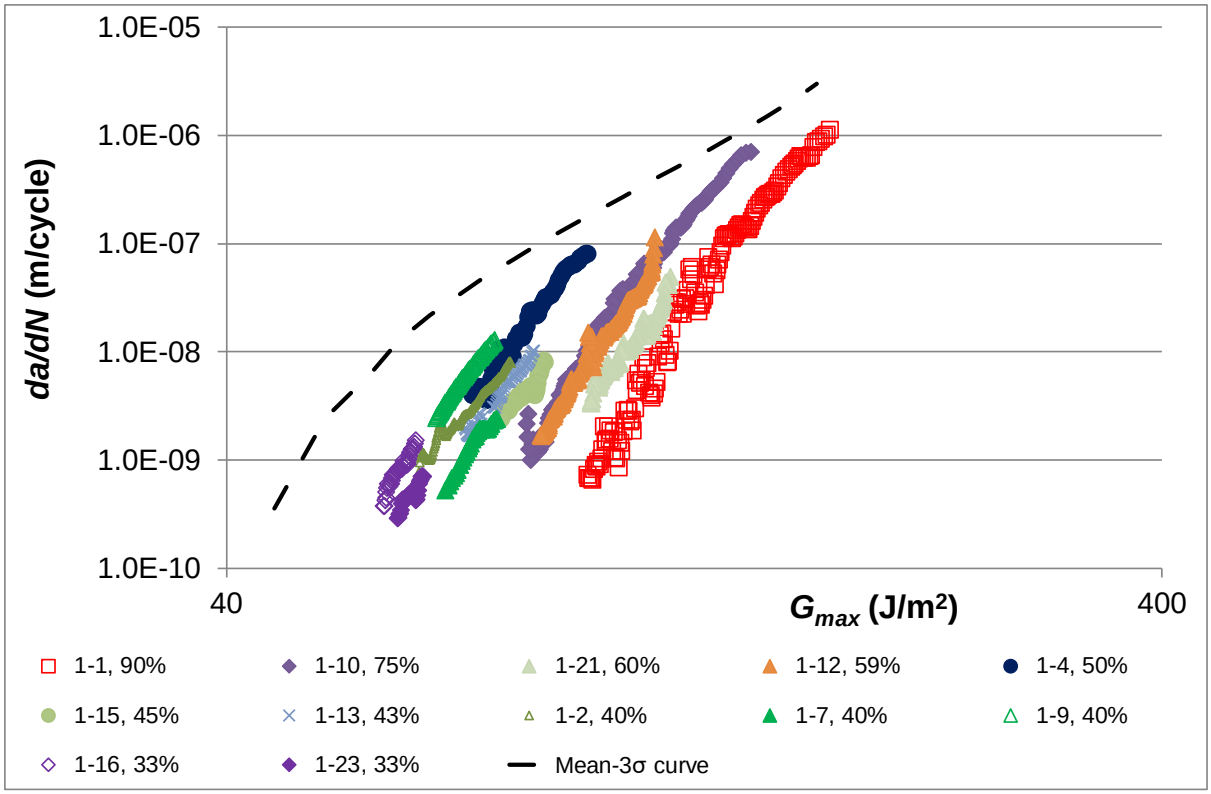

Figure 21. Various *da*/*dN* v G_{max} plots for IM7/8552 CFRP, from [17].

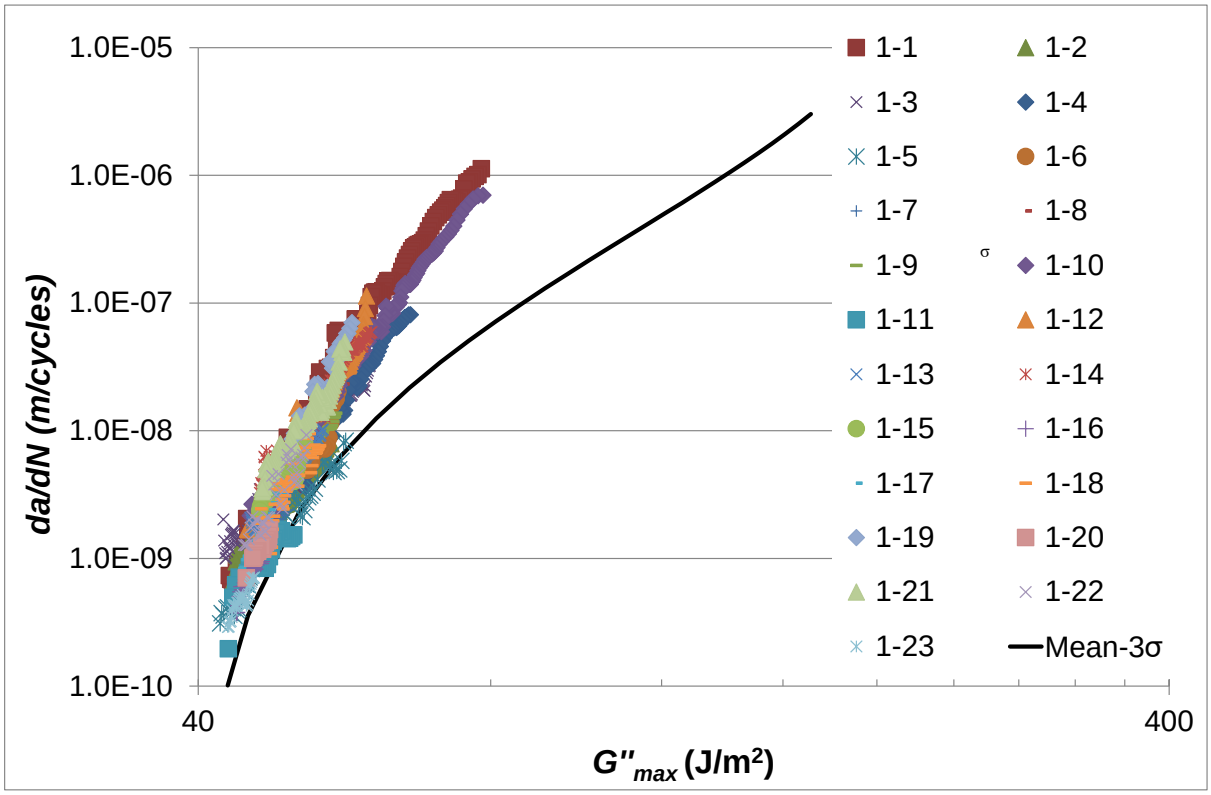

Figure 22. Comparison of the various scaled *da*/*dN* versus G''_{max} plots for the IM7/8552 CFRP tests.

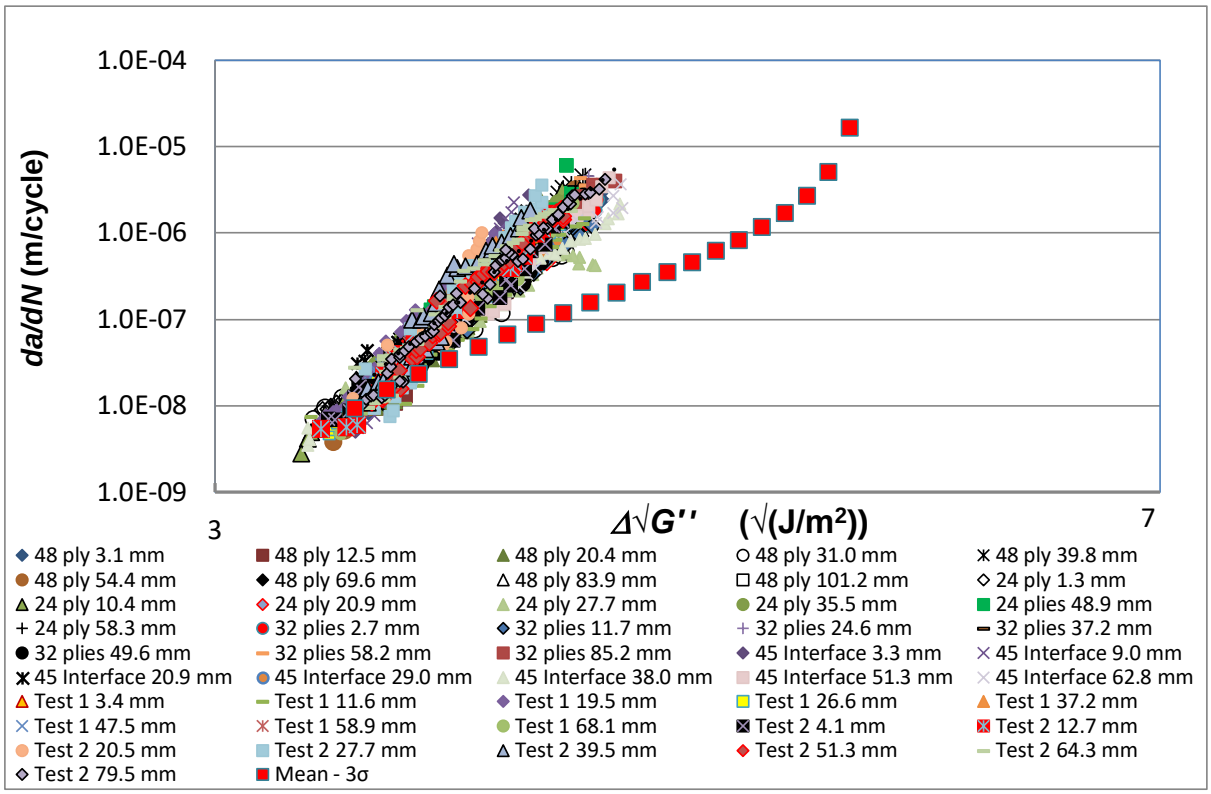

Figure 23. Comparison of the various scaled *da*/*dN* versus $\Delta\sqrt{G''}$ plots for the M30SC/DT120 CFRP test data shown in Figure 3.

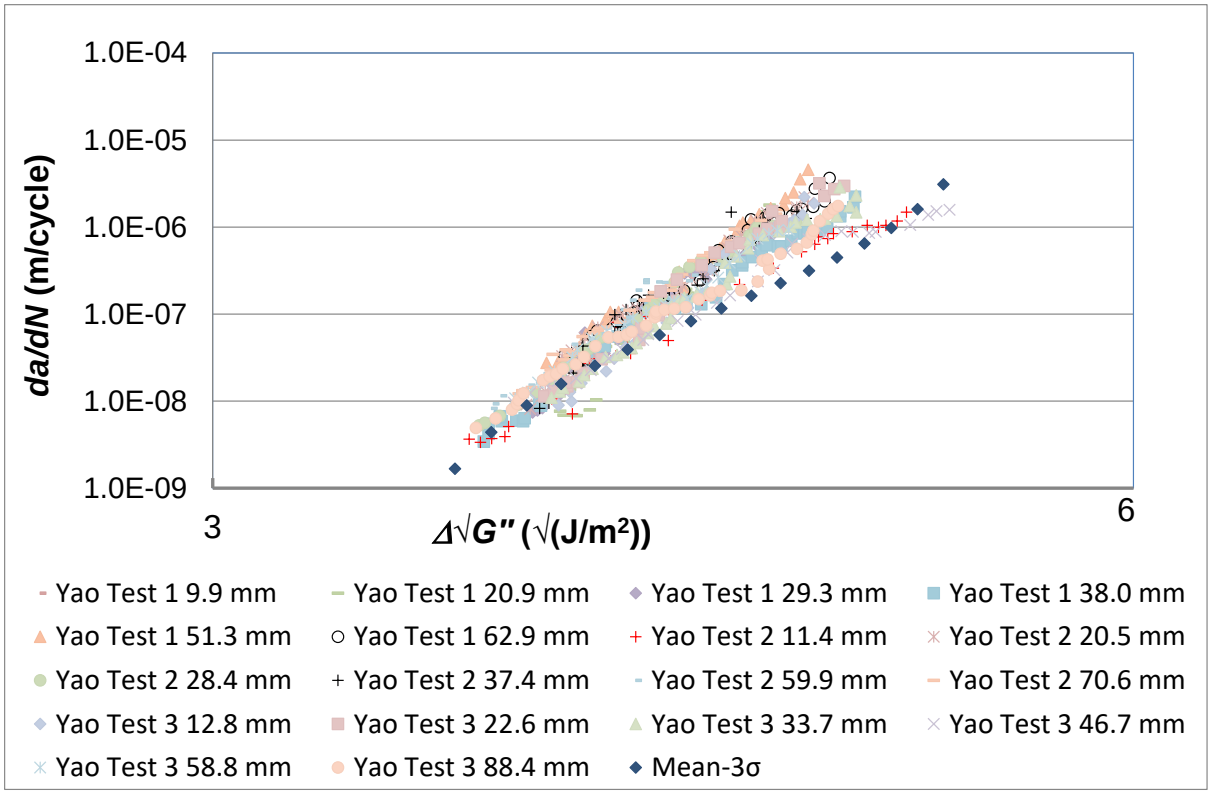

Figure 24. Comparison of the various scaled *da*/*dN* versus $\Delta\sqrt{G''}$ plots for the M30SC/DT120 CFRP test data shown in Figure 4.

Table 1. Values of the terms employed in Equation (3) and the 'mean-3σ' threshold, from [18].

Term	Value
D	1.73×10^{-8}
n	2.22
$\Delta\sqrt{G_{thr}}$ - 3 standard deviations	3.3 $\sqrt{(J/m^2)}$
$G_C = G_{C0}$ - 3 standard deviations	115 J/m^2

Table 2. Values of ΔK_{th} used in the various examples.

Material and reference	Type of test and R ratio	Fatigue threshold^{+} ΔK_{th} (MPa$\sqrt{m}$)
7050-7451 [64]	NASA K_{max}	1.2
	CT R = 0.1	2.0
	CT R = 0.5	1.5
	MT R = 0.2	1.5
	MT R = 0.1	1.7
	MT R = 0.7	1.0
2024-T3 [67]	-1.0	4.40
	0.0	2.95
	0.5	2.10
	0.7	1.95
2324-T39 [65]	-1.0	10.0
	0.1	4.60
	0.3	3.82
	0.5	2.84
	0.7	2.12
7075-T6511 [69]		
CT	0.1	1.70
SENT	0.1	2.00
6013-T651 [66]	-1.0	9.45
	0.0	4.40
	0.3	3.60
	0.5	2.60
	0.7	2.80
Cold-rolled metastable austenitic stainless steel [68]		
	0.1	7.00
	0.5	4.50

Table 3. Values of ΔK_{th} used in Figure 19.

R ratio and build direction	ΔK_{th} (MPa$\sqrt{}$m)
R = 0.1, perpendicular	8.2
R = 0.1, parallel	7.3
R = 0.5, perpendicular	6.0
R = 0.5, parallel	5.2
R = 0.7, perpendicular	4.7

Table 4. Values of $G_{max.th}$ used in Figure 20.

'Test'	$G_{max.th}$ (J/m^2)
90% G_c, Test 1	62
90% G_c, Test 2	60
90% G_c, Test 3	53
50% G_c, Test 1	46
50% G_c, Test 2	50
40% G_c, Test 1	46
40% G_c, Test 2	41
30% G_c, Test 1	37
30% G_c, Test 2	36
30% G_c, Test 3	39

Table 5. Values of $G_{max.th}$ used in Figure 22.

'Test'	$G_{max.th}$ (J/m^2)
1-1	89
1-2	58
1-3	68
1-4	58
1-5	66
1-6	56
1-7	62
1-8	67
1-9	55
1-10	73
1-11	54
1-12	76
1-13	63
1-14	75
1-15	67
1-16	53
1-17	67
1-18	60
1-19	83
1-20	53
1-21	83
1-22	68
1-23	56

Table 6. Values of $\Delta\sqrt{G_{th}}$ used in Figure 23.

Ply configuration and (a_p-a_0) in mm	$\Delta\sqrt{G_{th}}$ $\sqrt{(J/m^2)}$
$[(0)_{16}//(0)_{16}]$ ('Test 1')	
3.4	5.0
11.6	7.5
19.5	8.2
26.6	8.6
37.2	9.0
47.5	9.2
59.8	9.7
68.1	10.2
$[(0)_{16}//(0)_{16}]$ ('Test 2')	
4.1	6.2
12.7	6.8
20.5	8.2
27.7	8.5
39.5	9.4
51.3	9.4
64.3	10.1
79.5	10.1
32 ply $[(0)_{16}//(0)_{16}]$	
2.7	6.2
11.6	7.0
24.6	8.0
37.2	8.6
49.6	9.5
58.1	9.6
85.2	10.0
$[(0)_{24}//(0)_{24}]$ (48 plies, thickness = 7.5 mm)	
3.1	5.8
12.5	6.3
20.4	6.9
31	8.0
39.8	8.6
54.4	9.0

69.6	9.9
83.9	9.9
101.2	9.9
$[(0)_{12}//(0)_{12}]$ (24 plies, thickness = 3.75 mm)	
1.3	6.5
10.4	7.4
20.9	8.1
27.7	7.5
35.5	9.1
48.9	9.3
58.3	9.6
$[(\pm 45/0_{12}/\mp 45)//(\pm 45/0_{12}/\mp 45)]$	
3.3	5.4
9	7.3
20.9	10.1
29	10.4
38	10.8
51.3	11.8

Table 7. Values of $\Delta\sqrt{G_{th}}$ used in Figure 24.

'Test' and (a_p-$a_{0)}$	$\Delta\sqrt{G_{th}}$ $\sqrt{(J/m^2)}$
Test 1, 9.9 mm	6.9
Test 1, 20.9 mm	8.6
Test 1, 29.3 mm	9.0
Test 1, 38.0 mm	9.5
Test 1, 51.3 mm	10.7
Test 1, 62.9 mm	10.7
Test 2, 11.4 mm	5.7
Test 2, 20.5 mm	7.9
Test 2, 28.4 mm	9.4
Test 2, 37.4 mm	10.3
Test 2, 59.0 mm	10.7
Test 2, 70.6 mm	10.9
Test 3, 12.8 mm	6.0
Test 3, 22.6 mm	7.6
Test 3, 33.7 mm	8.2
Test 2, 46.7 mm	8.2
Test 2, 58.8 mm	10.3
Test 2, 88.4 mm	10.7